Inhalation Toxicology, 14:789–834, 2002

0895–8378/02 $12.00 + .00
DOI: 10.1080/0895837029008464 7

Taylor & Francis
healthsciences

PHYSIOLOGICALLY BASED PHARMACOKINETIC MODELING OF STYRENE AND STYRENE OXIDE RESPIRATORY-TRACT DOSIMETRY IN RODENTS AND HUMANS

Ramesh Sarangapani, Justin G. Teeguarden

The K. S. Crump Group, Inc., Research Triangle Park, North Carolina, USA

George Cruzan

ToxWorks, Bridgeton, New Jersey, USA

Harvey J. Clewell

ENVIRON International Corporation, Ruston, Louisiana, USA

Melvin E. Andersen

Department of Environmental Health, Colorado State University, Ft. Collins, Colorado, USA

Styrene (ST) is widely used to manufacture resins, glass-reinforced plastics, and a number of commercially important polymers (Miller et al., 1994). Chronic ST inhalation studies in rodents have demonstrated unique species specificity in the resulting pulmonary toxicity and carcinogenicity. Increased incidences of pulmonary bronchioloalveolar tumors have been observed in mice, but not in rats. No other tumor type was increased significantly in either species. Clara cells lining the respiratory epithelium metabolize ST to styrene 7,8-oxide (SO), which is cytotoxic and weakly genotoxic. Rodent species show marked differences in the distribution and regional density of Clara cells within the respiratory tract, as well as in their capacity to produce and eliminate SO. A mode of action-based physiologically based pharmacokinetic (PBPK) model was developed to predict the concentration of ST and SO in blood, liver, and the respiratory-tract tissues, particularly in terminal bronchioles (target tisue), in order to conduct interspecies extrapolations and determine the extent to which there is a pharmacokinetic basis for the observed species specificity. This PBPK model has a multicompartment description of the respiratory tract and incorporates species-specific quantitative information on respiratory-tract physiology, cellular composition, and metabolic capacity. The model is validated against multiple data sets, including blood, liver, and whole lung tissue concentration of ST and SO following multiple routes of exposure. The trend in neoplastic incidences in mice correlated well with model-estimated SO concentration in the terminal bronchioles. The PBPK model predicts a 10-fold lower SO concentration in the terminal bronchioles in rats compared to mice, which is

Received 10 January 2001; accepted 11 February 2002.

We thank the Styrene Information and Research Center for support of this work. We also acknowledge and thank Drs. Johannes Filser (GSF, Germany), György Csanày (GSF, Germany), Tim Fennell (CIIT Centers for Health Research), and Michele Medinsky (ToxCon, NC) for their critical evaluation of an earlier draft of this article.

Address correspondence to Dr. George Cruzan, ToxWorks, 1153 Roadstown Road, Bridgeton, NJ 08302, USA. E-mail: toxworks@aol.com

consistent with the observed species sensitivity to the development of respiratory-tract neoplasms. The model-based analysis suggests that humans would be expected to be 100-fold less sensitive to ST-inducted lung tumors than mice, based on pharmacokinetic differences. Pharmacodynamic factors are also expected to contribute to species sensitivity, potentially augmenting pharmacokinetics-based differences.

Styrene (ST) is widely used to manufacture resins, glass-reinforced plastics, and a number of commercially important polymers (Miller et al., 1994). The most substantial human exposure to ST occurs via the inhalation route in occupational settings. The database describing the toxicity, metabolism, and toxicokinetics of styrene is extensive (McConnell & Swenberg, 1994; Sumner & Fennell, 1994). Epidemiologic studies of ST exposed workers, recently reviewed, conclude there is inadequate evidence of carcinogenicity of ST in humans (SIRC, 1999). However, pneumotoxicity in mice and mild hepatotoxicity (only at high dose) in rats have been observed in studies using rodents (Bond, 1989; SIRC, 1999). Recently the Styrene Information and Research Center (SIRC) conducted subchronic and chronic inhalation studies exposing both rats and mice to various concentrations of ST. No evidence of treatment-related increases in any type of tumor was observed in rats, compared to controls, at the end of the 2-yr inhalation study (Cruzan et al., 1998). However, the chronic inhalation study with mice resulted in statistically significantly increased incidences of bronchioloalveolar tumors in both male and female mice at the end of 2 yr, but not after 12 or 18 mo (Cruzan et al., 2001). Decreased eosinophilia in terminal bronchioles, focal crowding, and bronchiolar hyperplasia, eventually extending into alveolar ducts, were seen at progressively lower exposure concentrations in mice sacrificed at 12, 18, and 24 mo (Cruzan et al., 2001).

Metabolic activation of ST to styrene 7,8-oxide (SO) is carried out by microsomal P-450s and produces both an *R* and an *S* enantiomer. SO is both cytotoxic and carcinogenic, with the *R*-enantiomer being somewhat more cytotoxic than the *S*-enantiomer (Gadberry et al., 1996). SO is believed to be the proximal toxicant responsible for toxicity and carcinogenicity observed following exposure to ST (Bond, 1989; Carlson, 1998; Sumner & Fennell, 1994). SO is cleared (detoxified) by microsomal epoxide hydrolase (EH)-mediated hydrolysis and glutathione (GSH) conjugation by cytosolic glutathione *S*-transferases (GSTs). These enzyme systems are present in several tissues, including the liver and lungs of rats, mice, and humans (Baron & Voigt, 1990; Mace et al., 1998; Mendrala et al., 1993; Pacifici et al., 1987; Schladt et al., 1988; Waechter et al., 1988). Species differences in the metabolic activity and stereospecificity of these enzymes has been demonstrated (Bond, 1989; Sumner & Fennell, 1994) and has led to the hypothesis that the observed species differences in toxicity can be attributed to species differences in toxicokinetics of ST and SO. This hypothesis can be tested by evaluating the effect of species differences in anatomical, physiological, and metabolic parameters on SO target tissue dose using a physiologically based pharmacokinetic (PBPK) model.

The U.S. EPA proposed guidelines for carcinogen risk assessment promote the incorporation of mode of action (MOA) information and the use of physiologically based pharmacokinetic (PBPK) models when conducting high-dose to low-dose and interspecies extrapolation (U.S. EPA, 1996, 1999). A significant amount of mechanistic and toxicokinetic information has been collected on ST and its metabolites in rodents and humans. The principle objective of this article was to develop an MOA-based PBPK model for inhaled ST that integrates relevant mechanistic and toxicokinetic information and is capable of describing the relationship between exposure and target tissue dose of ST and its reactive intermediate SO in rodents and humans. Additional objectives were to conduct an analysis of *R*-SO and *S*-SO target tissue dose using the PBPK model and evaluate the extent to which there is a pharmacokinetic basis for the species-specific carcinogenic response following chronic inhalation exposure to ST.

METHODS

A number of models have been developed to describe the disposition and metabolism of inhaled ST. Ramsey and Andersen (1984) developed a physiologically based description of the inhalation pharmacokinetics of ST in rats to explain the relationship between its blood concentration and inhaled air concentration. More recently, Csanady et al. (1994) developed a PBPK model to describe the blood/tissue concentration time course of ST and SO in the rat, mouse, and human following multiple routes of administration. However, neither model was designed to incorporate metabolic production and clearance of SO in the respiratory tract or to treat the respiratory tract as a target organ. Here, we have extended this previous work by incorporating a detailed multicompartment description of the respiratory tract with a compartment specific to the terminal bronchiolar region, where ST-mediated toxicity is observed.

Respiratory-Tract Anatomy and Cell Composition

Based on its anatomical location and function, the respiratory tract can be broadly divided into four regions: the upper airways, the conducting airways, the transitional airways, and the pulmonary airways (i.e., gas exchange region). The upper airways consist of the nasal cavity, and the conducting airways comprise the rest of the anterior respiratory tract not involved in gas exchange. In rodents, the most distal conducting airways are the terminal bronchioles, which abruptly open into the alveoli (Parent, 1992). In humans, the transition between the conducting and gas-exchange region is formed by the respiratory bronchioles (ICRP, 1994). The respiratory bronchioles in humans span two to four generations, containing a variable number of alveolar sacs, and form a gradual transition between the conducting and gas-exchange region. In this report the term *transitional bronchioles* refers to the terminal bronchiolar region in rodents and the respiratory bronchiolar region in humans.

The most common cell types of the conducting airways are the ciliated and basal cells, while the nonciliated Clara cells dominate the transitional airways. In mouse, rat, and human the surface of the pulmonary airways (alveoli) is lined by a single-cell-thick continuous layer of Type I and Type II alveolar epithelial cells. The regional distribution and fractional density of Clara cells is significantly different between mice, rats, and humans. The number and size of Clara cells in the rat lung have been determined by quantitative morphometric analysis, and these studies report a total of 17.3×10^6 Clara cells in the rat lung, with approximately 42% of the total Clara cells confined to the terminal bronchioles (Mercer et al., 1994). In the mouse, Clara cells are found throughout the conducting airways, with the highest density in the terminal bronchioles (Pack et al., 1981; Plopper et al., 1980b, 1992). Values of the Clara cell fractional density have been reported in different regions of the mouse airway including trachea (36%), primary bronchi (47%), lobar bronchi (61%), axial bronchi (36%), and terminal bronchioles (average, 78.5%) (Pack et al., 1981; Parent, 1992; Plopper et al., 1980b, 1992).

In contrast to the mouse and rat, Clara cells in the human are not present in the bronchi and terminal bronchioles but are confined primarily to the respiratory bronchioles (Parent, 1992), which comprise approximately three generations immediately distal to the terminal bronchioles (ICRP, 1994). The number and size (height, volume) of Clara cells in the human bronchioles have been determined by quantitative morphometric analysis (Mercer et al., 1994), and these reports indicate a total of 1.38×10^9 Clara cells in the human lung, with 85% confined to the respiratory bronchioles. The fractional volume density of Clara cells in the human respiratory bronchioles, based on the ratio of Clara cell volume to total epithelial cell volume in this region, is approximately 7.5% (Mercer et al., 1994).

Mode of Action

The construction of the respiratory-tract compartments in the PBPK model was guided by a mode of action for ST induced pulmonary carcinogenicity. A substantial amount of evidence has been collected that characterizes the metabolic basis of cell- and species-specific toxicity of ST in the lung, the relative genotoxic potential of ST, and the incidence, regional localization, and cell type of precursor lesions and neoplasms observed in mice after short-term and chronic exposure to ST. In the rodent lung, tumors typically arise from one of two cell types: either the nonciliated bronchiolar (Clara) cell or the Type II cells (Boorman et al., 1990; Stoner, 1998). Human and rodent lungs contain both these cell types, with unique species-related differences in the density and distribution of Clara cells (Plopper et al., 1980a). Damage to both cell types has been observed after exposure to pulmonary toxicants (Boorman et al., 1990). The pathobiology of ST-induced bronchioloaveolar tumors constructed from bioassay and other mechanistic studies does not conclusively identify one of these cell types as the target cell for carcinogenesis.

The time course of pulmonary effects observed in Clara cells from the chronic ST inhalation study in mice supports a progression of events in the development of bronchioloalveolar carcinomas that is consistent with descriptions of multistage lung carcinogenesis (Boorman et al., 1990; Stoner, 1998) and dominated by a nongenotoxic MOA (Green, 1999): Clara-cell toxicity (decreased eosinophilia of cells in the terminal bronchiole, focal crowding, loss of apical cytoplasm), followed sequentially by increased cell proliferation, focal crowding (Clara cell), and bronchiolar epithelial hyperplasia (Clara cell).

A similar, parallel time course of cellular events cannot be constructed for Type II cells directly from experimental data. However, hyperplastic lesions and adenomas/carcinomas of the bronchioloalveolar region, which stain immunohistochemically for surfactant produced by normal type II cells, but not normal Clara cells, occur at a greater incidence in ST exposed mice than in controls (Cruzan et al., 2001). Thus, ST appears to exacerbate the development of spontaneous hyperplastic lesions and tumors in CD-1 mice.

The equivocal genotoxic potential of ST and weak genotoxic potential of its more reactive metabolite SO do not support a genotoxicity dominated MOA for ST-induced tumors (Bond, 1989; SIRC, 1999). This is substantiated by the observation that unlike ST, genotoxic compounds frequently give rise to tumors at multiples sites in more than one test species (U.S. EPA 1996, 1999). Tumors restricted to single species and/or late onset of tumors that are primarily benign and at sites with a high historical background incidence point to a growth-related MOA (U.S. EPA 1996, 1999). The incidence of ST carcinogenicity (nontumorigenic in rats, and tumorigenic for a single site in mice at the end of a 2-yr study) is consistent with this pattern produced by nongenotoxic compounds. While a genotoxic contribution to the ST MOA cannot be excluded, the available data supports the hypothesis that the MOA of ST carcinogenicity contains a strong nongenotoxic component.

Although toxicological data are not definitive with regard to a target cell, they are sufficient to support a strong hypothesis regarding the MOA for ST-induced lung tumors in mice, which can be applied similarly to the two potential target cells: Clara cells and Type II cells. The proposed MOA for ST-induced bronchioloalveolar tumors is that SO binds to non-DNA nucleophiles (SIRC, 1999), and only weakly to DNA, causing cytotoxicity and sustained regenerative proliferation of Clara cells (Cruzan et al., 2001), which precedes development of focal hyperplasias. In response to the continued promotional stimulus caused by the observed Clara cell cytotoxicity following chronic exposure to ST, some bronchioloalveolar hyperplasias develop into bronchioloalveolar adenomas, a small fraction of which progress into bronchioloalveolar carcinomas. Accumulation of specific genetic lesions required for malignant conversion is dominated by replicative errors during sustained regenerative proliferation rather than the weak genotoxic activity of ST.

TARGET TISSUE DOSIMETRY

Based on the proposed MOA, two tissue dose metrics can be explored as candidates for interspecies and high-to-low dose extrapolations of target tissue concentrations using the PBPK model; one is cell specific and the other region specific. The use of a cell-specific dose metric is based on the assumption that the bronchioloalveolar tumors arise from the Clara cells in the terminal bronchioles. This dose metric is cell specific, and best reflects MOA considerations if Clara cells are established as the cell of origin for the pulmonary tumors. The cell-specific dose metric is representative of SO concentration in Clara cells within a homogeneous cell population, and is governed by enzyme activity in the Clara cells. This dose metric does not apply to individual Clara cells that exist in a heterogeneous cell population, since it does not account for lateral transport of SO to neighboring non-Clara cells.

Pulmonary metabolism of ST to SO is limited to Clara cells (Hynes et al., 1999). Clara cells are concentrated in the terminal bronchioles of the lung, which are the most distal branches of the conducting airways that open into the alveolar region. The alveoli are lined by Type I and Type II alveolar epithelial cells (Boorman et al., 1990). This junction between the terminal bronchioles and alveolar ducts is a region where Clara cells are in the closest proximity to alveolar Type II cells, although normally separated by a few Type I cells. It is possible that the proximity of Clara cells and Type II cells in this region could facilitate the lateral transport of SO produced predominantly in the Clara cells to the alveolar Type II cells.

The use of region-specific dose metric is based on the assumption that the bronchioloalveolar tumors arise at the distal end of the terminal bronchioles, but that the cell of origin is either Clara or Type II. This dose metric is representative of the SO concentration in a mixed cell population, and is governed by the average enzyme activity in the terminal bronchioles. The concentration of total SO and *R/S* SO will be estimated in this tissue volume containing a species-specific density of Clara cells in close proximity to Type II cells. The region-specific dose metric provides an averaged concentration in the region where Clara cell metabolism may contribute significantly to Type II cell SO exposure and is roughly consistent with the location of the observed tumors.

PBPK Model Structure

Previous PBPK models for ST have described the lung compartment as a single uniform tissue and described gas-exchange dynamics at the portal of entry using closed-form equilibrium relationships (Csanady et al., 1994; Ramsey & Andersen, 1984). In the current PBPK model, the four regions of the lung described in the previous section are modeled as separate compartments, with special emphasis on the characterization of the transitional bronchiolar compartment, the primary target site for ST-induced lung tumors and the region richest in the metabolically active Clara cell. The

overall PBPK model has a nested architecture with a model for the parent chemical and a linked submodel for the metabolite SO (Figure 1). Both models have a similar tissue compartmentalization that includes a four-compartment respiratory tract and tissues important for systemic clearance and storage. The systemic tissues in the body are grouped into four compartments: liver, fat, richly perfused tissue, and poorly perfused tissue. Metabolic activation of ST by cytochrome P-450-catalyzed epoxidation and

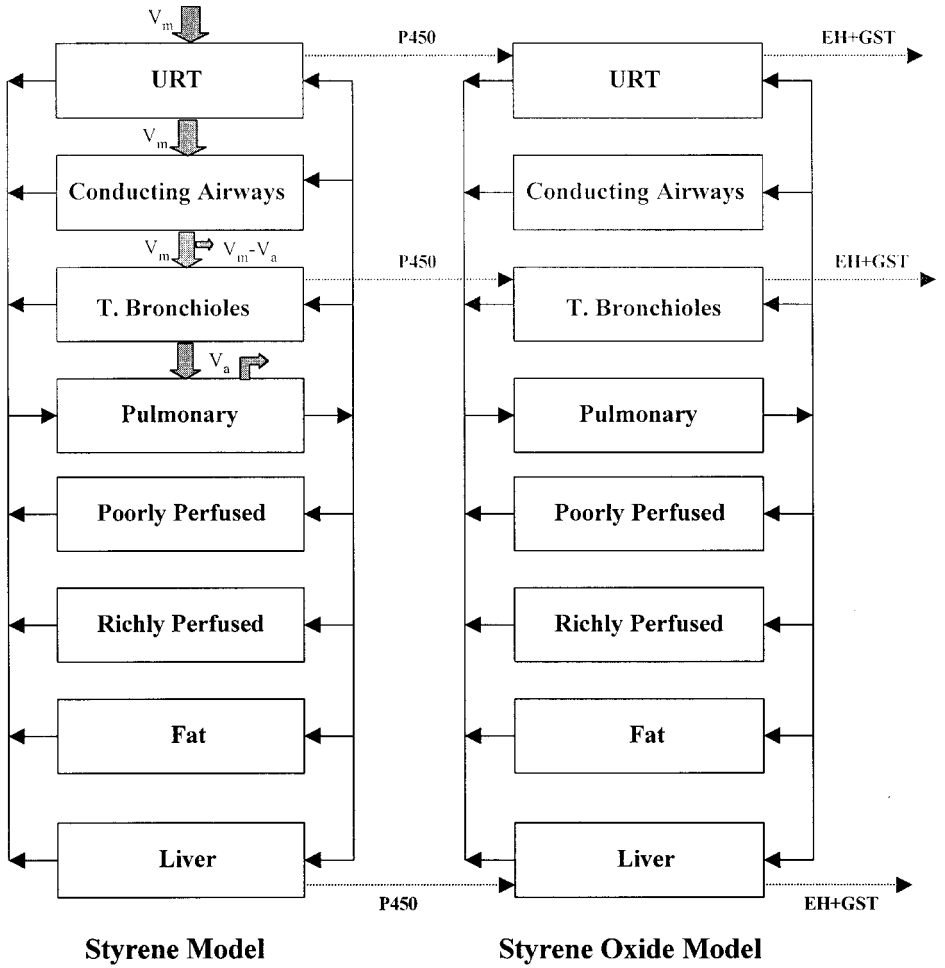

FIGURE 1. Schematic of the PBPK model used to study absorption, distribution, and metabolism of ST and SO via the inhalation route. The PBPK model for ST and its metabolite, SO, has a nested architecture with a model for the parent chemical and a linked submodel for the metabolite SO. Both PBPK models have a similar tissue compartmentalization that include the respiratory-tract tissue, liver, fat, richly perfused tissue, and poorly perfused tissue. Metabolic activation of ST by cytochrome P-450-catalyzed epoxidation and the detoxication of SO by EH and GST are modeled as occurring in the liver and selected regions of the lung. SO formed in any given tissue compartment in the ST model is passed to the corresponding tissue compartment in the SO submodel for further transport and metabolism.

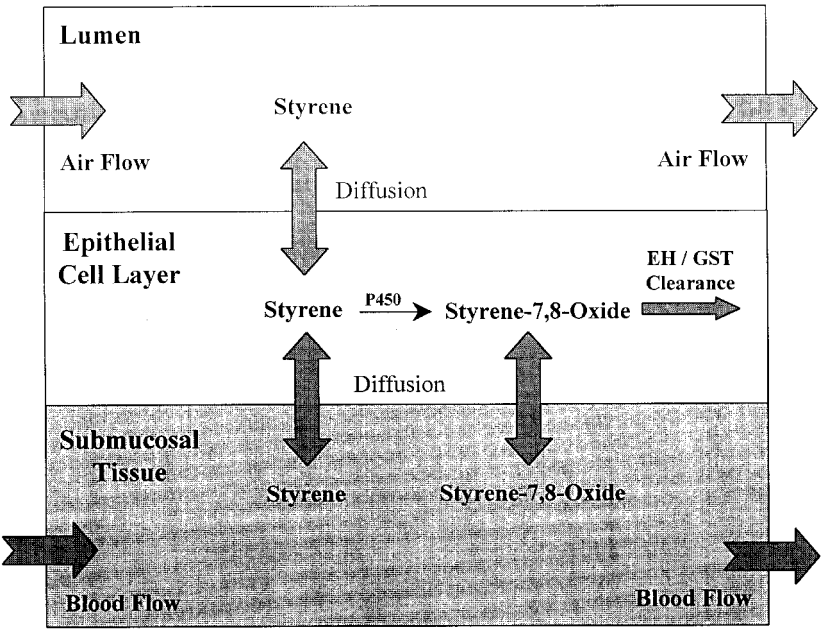

FIGURE 2. Schematic of an airway tissue compartment showing the three-layered substructure in the respiratory tract, with the various transport and metabolic pathways for ST. Inhaled ST is absorbed at the lumen–tissue interface and then diffuses into the epithelial cell layer where it is metabolized to SO, depending on the activity of the P-450 enzyme system. The SO is further metabolized in the epithelial tissue by EH and GST. The remaining ST and SO in the epithelial tissue diffuses into the submucosal tissue. ST and SO diffusing into the submucosal tissue are assumed to equilibrate rapidly with capillary blood and are cleared by the venous flow to the general blood circulation.

the detoxication of SO by EH and GST are modeled as occurring in the liver and selected regions of the lung. All the metabolic steps are assumed to be irreversible, and SO formed in the parent model in any given tissue compartment is passed to the corresponding tissue compartment in the metabolite submodel for further transport and metabolism (Figure 1).

The respiratory tract has a complex and variable structure comprising a lumen for air passage that is surrounded by epithelium and submucosa tissue layers. To reflect the architecture of the respiratory tract tissue, the tissue compartments representing the nasal cavity, conducting airways, and transitional airways are divided into a three-layered substructure consisting of a lumen, epithelium, and a submucosal tissue layer (Figure 2). Although the epithelium and the submucosa are composed of a number of morphologically distinct cell types, these multiple cell types are represented by a single composite epithelial and submucosal tissue layer in the PBPK model (Figure 2). In each of the respiratory-tract compartments, the lumen is ventilated by the inhaled air delivered from the previous compartment and only the submucosal tissue layer is assumed to have blood perfusion that clears ST and SO. The epithelium forms the target tissue and contains the enzymes for biotransformation of ST and SO.

A fraction of the ST in the inhaled airstream is absorbed in the anterior regions of the respiratory tract, namely, the nasal cavity, conducting airways, and transitional airways (Morris, 2000). Inhaled ST is absorbed at the lumen-tissue interface and then diffuses into the epithelial cell layer, where it is metabolized to SO, depending on the P-450 activity. SO is further metabolized in the epithelial tissue by EH and GST. The remaining ST and SO in the epithelial tissue diffuses into the submucosal tissue. ST and SO diffusing into the submucosal tissue are assumed to equilibrate rapidly with capillary blood and are cleared by the venous flow to the general blood circulation. The model incorporates a mass transfer coefficient at the lumen–tissue interface that governs the net flux of ST from the lumen into the epithelial tissue by diffusional transport. The diffusional flux of ST and SO across the epithelial and submucosal layers is characterized by an intercompartmental diffusional resistance term. Ventilation is assumed to be unidirectional in this model. Air flow rate in the upper and conducting airways is assumed equal to the minute ventilation, and the flow rate in the transitional and pulmonary airways is assumed equal to the alveolar ventilation. A portion of the volumetric flow, equivalent to dead-space ventilation, exits the respiratory tract from the conducting airways (Figure 1). Analytical expressions that describe the transport of an inhaled chemical across the lumen and tissue subcompartments in the upper, conducting, and transitional airways have been derived elsewhere (Andersen et al., 1999; Bogdanffy et al., 1999) and are only summarized here (Table 1).

ST that penetrates into the gas-exchange region is assumed to equilibrate rapidly with arterial blood exiting the lung. Arterial blood leaving the lung is distributed to seven main tissue groups: fat, liver, anterior lung tissues (i.e., upper, conducting, and transitional airways), richly perfused tissues, and poorly perfused tissues. The liver, nasal cavity, and transitional bronchioles are the primary tissues involved in the biotransformation of ST and SO, and the remaining tissues act as storage depots for ST and its metabolites depending on their respective blood:tissue partition coefficient and perfusion rate. Metabolism of ST and SO in other tissues is not considered in this model because of their low metabolic capacity (Bond, 1989; SIRC, 1999), which will not contribute significantly to blood, or target tissue concentrations of SO. The concentration of ST and SO exiting any given tissue compartment is determined by the compartment-specific clearance kinetics and tissue:blood partition coefficient. The mixed mean ST and SO concentrations in the venous blood are determined as the flow averaged concentration exiting all the tissue compartments. The mixed venous blood returns to the lung at a flow rate equal to the cardiac output.

The kinetics of the biotransformation of ST in the liver and the respiratory tract tissues are modeled according to the previously published works of Johanson and Filser (1993) and Csanady et al. (1994). The oxidation of ST by P-450 and the hydrolysis of SO by EH are represented by a saturable process with Michaelis–Menten kinetics. The cytochrome P-450 enzymes and EH are located within the endoplasmic reticulum and GST is present in

TABLE 1. Mass Balance Equations in the Styrene Model for the Respiratory-Tract Tissues and Hepatic Tissue and the Overall Mass Balance in the Blood Compartment

Governing mass balance equations for parent species in liver and respiratory-tract compartments	
RT lumen [ST]	$V_l \frac{dC_l}{dt} = \dot{V}_m(C_{in} - C_l) - K_{at}SA_x\left(C_l - \frac{C_t}{H_{t:a}}\right)$
Epithelium [ST]	$V_t \frac{dC_t}{dt} = K_{at}SA_x\left(C_l - \frac{C_t}{H_{t:a}}\right) - K_{tb}SA_x\left(\frac{C_t}{H_{t:b}} - \frac{C_x}{H_{t:b}}\right) - \frac{V_{m1}C_t / H_{t:b}}{K_{m1} + C_t / H_{t:b}}$
Submucosa [ST]	$V_x \frac{dC_x}{dt} = K_{tb}SA_x\left(\frac{C_t}{H_{t:b}} - \frac{C_x}{H_{t:b}}\right) - \dot{Q}_x(C_{art} - C_x / H_{t:b})$
Liver [ST]	$V_{li} \frac{dC_{li}}{dt} = Q_{li}(C_{art} \; C_{li} / H_{t:b}) - \frac{V_{m1}C_{li} / H_{t:b}}{K_{m1} + C_{li} / H_{t:b}}$
Governing mass balance equations for epoxide in liver and respiratory tract	
ER [SO]	$V_{li} \frac{dE_{er}}{dt} = \frac{V_{m1}C_{li} / H_{t:b}}{K_{m1} + C_{li} / H_{t:b}} - K_{ec}\left(\frac{E_{er}}{H^{SO}_{t:b}} - \frac{E_{cy}}{H^{SO}_{t:b}}\right) - \frac{V_{m2}E_{er} / H^{SO}_{t:b}}{K_{m2} + E_{er} / H^{SO}_{t:b}}$
CY [SO]	$V_{li} \frac{dE_{cy}}{dt} = K_{ec}\left(\frac{E_{er}}{H^{SO}_{t:b}} - \frac{E_{cy}}{H^{SO}_{t:b}}\right) - \dot{Q}_x\left(E_{art} - \frac{E_{cy}}{H^{SO}_{t:b}}\right) - \frac{V_{m3}E_{cy}GSH_{li}}{K_mE_{cy} + K_mE_{cy} + K_{m3}GSH_{li} + E_{cy}GSH_{li}}$
[GSH]	$V_{li} \frac{dGSH_{li}}{dt} = K_{GSH}(GSH_B - GSH_{li}) - \frac{V_{m3}E_{cy}GSH_{li}}{K_mE_{cy} + K_{m3}GSH_{li} + E_{cy}GSH_{li}}$
Overall mass balance equation for parent species and epoxide in blood compartment	
Blood [ST]	$\dot{Q}_cC_{ven} = \dot{Q}_{li}C_{li} + \dot{Q}_fC_f + \dot{Q}_{rt}C_{rt} + \dot{Q}_{pt}C_{pt} + \dot{Q}_xC_x$
Blood [SO]	$\dot{Q}_cE_{ven} = \dot{Q}_{li}E_{cy} + \dot{Q}_fE_f + \dot{Q}_{rt}E_{rt} + \dot{Q}_{pt}E_{pt} + \dot{Q}_xE_x$

Note. C_l, C_t, C_x—styrene concentration in respiratory tract lumen, tissue, and submucosa, respectively. C_{li}, C_f, $C_{rt/pt}$—styrene concentration in liver, fat, richly and poorly perfused tissues, respectively. E_{er}, E_{cy}—epoxide concentration in liver endoplasmic reticulum and cytosolic fraction, respectively. $E_fE_{rt}E_{pt}$—epoxide concentration in fat, richly and poorly perfused tissues, respectively. $\dot{V}_m$, $\dot{Q}_c$—minute ventilation and cardiac output, respectively. $\dot{Q}_{li}$, $\dot{Q}_x$, $\dot{Q}_f$, $\dot{Q}_{rt/pt}$—blood flow rate to liver, lung, fat, richly and poorly perfused tissues, respectively. V_l, V_t, V_x, V_{li}respiratory tract lumen, tissue, and submucosa, and liver volumes, respectively. K_{at}, K_{tb}, K_{ec}—intercompartmental transfer coefficients. $H_{t:a}$, $H_{t:b}$, $H^{so}_{t:b}$—issue:air and tissue:blood partition coefficients for styrene and epoxide. V_{m1}, V_{m2}, V_{m3}—total metabolic capacity for P-450, EH, and GST activity, respectively. K_{m1}, K_{m2}, K_{m3}—affinity for P450, EH, and GST, respectively. K_{GSH}, GSH_B, GSH_{li}—GSH production rate, basal GSH, and liver GSH concentration, respectively.

the cytosol. The presence of the former two enzyme systems in close proximity within the microsomes results in first-pass metabolism of SO within the endoplasmic reticulum before it diffuses into the cytosol. To capture this first-pass effect, the epithelial cell layer is further partitioned into a cytoplasmic subcompartment and a microsomal subcompartment. The flux of SO from the endoplasmic reticulum to the cytosol is characterized by the product of the intercompartmental concentration gradient and a diffusional

clearance term. The diffusional clearance term was estimated by fitting the model to blood SO concentration following inhalation exposure to ST in rodents (Cruzan et al., 1998, 2001) and humans (Johanson et al., 2000). The conjugation of cytosolic SO with GSH is described by an ordered sequential "ping-pong" mechanism between GSH, SO, and GST, consistent with previous model formulations (Johanson & Filser, 1993). Because of its role as a cofactor in the reaction catalyzed by GST, GSH is depleted in liver and lung. In the model, the rate of change of amount of cytosolic GSH in the liver is described by a physiologically normal, background zero-order production rate, a conjugation-dependent depletion rate of GSH, and a first-order elimination rate reflecting the normal background degradation. Mass balance equations that describe the rate of production of SO from ST, elimination of SO, and kinetics of cytosolic GSH in the liver are derived elsewhere (Csanady et al., 1994) and are only summarized here (Table 1). A similar set of mass-balance equations is used in the lung tissue compartments. The model was coded using ACSL (Advanced Continuous Simulation Language, Aegis, Inc., Huntsville, AL). The model code will be made available upon request.

Model Parameterization of Physiological Constants

The various model parameters were obtained from the literature or inferred by fitting the model to PK data when direct measures where unavailable (Tables 2–4). Tissue volumes and blood perfusion rates to the various systemic organs (i.e., liver, fat, richly perfused, poorly perfused tissue), in all three species, were obtained from Brown et al. (1997). The blood:air partition coefficients for ST in rodents and humans were obtained from Gargas et al. (1989) and Sato and Nakajima (1979), and all the tissue:blood partition coefficients for ST and SO in rats were obtained from Csanady et al. (1994) and assumed to be the same in mice and humans. All the physicochemical and flow parameters are summarized in Table 2. Physiological parameters specific to the respiratory tract are summarized in Table 3.

Tissue volumes for the three anterior respiratory-tract compartments were estimated by multiplying the appropriate surface area with the tissue thickness. Nasal cavity surface area in laboratory animals and humans was obtained from Menache et al. (1997). Epithelial thickness in the nasal mucosa was obtained from Bogdanffy et al. (1998). The submucosal thickness was assumed to be approximately twice the epithelium thickness, based on histological sectioning (Matthew Bogdanffy, personal communication). Published data on the cardiac output to the nasal cavity in anesthetized rats and mice (Stott et al., 1983, 1986) and in resting human subjects (Paulsson et al., 1985) was used to parameterize the rodent and human models, respectively.

The surface area of the conducting and transitional airway in rodents and humans was estimated using standard lung models (ICRP, 1994; Oldham et al., 1994; Yeh et al., 1979) that quantify airway length and diameter on a generation-by-generation basis. In rodents, trachea through the 15th

TABLE 2. List of Physiological and Flow Parameters Used in the Styrene Model for Mouse, Rat, and Human

Parameter	Symbol	Mouse	Rat	Human	Reference
Body weight (g)	—	25	250	70,000	(Brown et al., 1997)
Tissue volume as fraction of body weight					
Liver volume	V_{li}	5.5	3.66	2.6	Same
Richly perfused volume	V_{rp}	10	12.34	8.5	Same
Poorly perfused volume	V_{pp}	70	70	60	Same
Fat volume	V_f	7	6.5	21.4	Same
Blood volume	V_b	7.5	7.5	7.5	Same
Minute ventilation (ml/min)	$\dot{V}_m$	24	150	15,000	(Brown et al., 1997; Morris 2000)
Pulmonary ventilation (ml/min)	$\dot{V}_m$	12–1[a]	75–110[a]	10,500	(Brown et al., 1997)
Cardiac output (ml/min)	$\dot{Q}_c$	14	110	5200	Same
Tissue blood flow as fraction of cardiac output					
Liver blood flow	$\dot{Q}_{li}$	15–30	15–30[a]	22.7	Same
Richly perfused blood flow	$\dot{Q}_{rp}$	48	28.7	43	Same
Fat blood flow	$\dot{Q}_f$	5.9	7	5.2	Same
UA blood flow	$\dot{Q}_x$	1.0	1.0	0.25	(Paulsson et al., 1985; Stott et al., 1983, 1986)
CA blood flow	$\dot{Q}_x$	0.5	2.1	0.75	(Brown et al., 1997)
TA blood flow	$\dot{Q}_x$	0.1	0.15	0.67	(Butler, 1992)
Partition coefficient					
ST blood:air	$H_{b:a}$	40	40	48	(Csanady et al., 1994; Gargas et al., 1989; Sato & Nakajima, 1979)
ST liver:blood	$H_{l:b}$	2	2	2	(Csanady et al., 1994; Ramsey & Andersen, 1984)
ST fat:blood	$H_{f:b}$	87	87	50	Same
ST tissue:blood	$H_{t:b}$	1.3	1.3	1.3	Same
SO blood:air	$H^{SO}_{b:a}$	2000	2000	2000	Same
SO liver:blood	$H^{SO}_{l:b}$	1	1	1	Same
SO fat:blood	$H^{SO}_{t:b}$	14	14	14	Same
SO tissue:blood	$H^{SO}_{t:b}$	0.6	0.6	0.6	Same
ST/SO tissue-phase diffusivity (cm^2/min)	D_t	0.0002	0.0002	0.0002	(Cussler, 1999)
ST/SO air-phase diffusivity (cm^2/min)	D_a	6	6	6	Same

Note. UA, upper airways; CA, conducting airways; TA, transitional airways.

[a]Shows the parameter range to fit all experimental datasets. Mean values are used for dose extrapolation. Mean value for alveolar ventilation rate in mice and rats is 18 and 110 ml/min, respectively. Mean values for hepatic blood perfusion in mice and rats is 16.1 and 18.3 ml/min, respectively (Brown et al., 1997).

generation was assumed to comprise the conducting airway, and the 16th airway generation was modeled as the terminal bronchiolar compartment. In humans, trachea through the 16th generation (i.e., including the terminal bronchioles) was assumed to comprise the conducting airway. The respiratory bronchioles, spanning 17th through the 19th generation, were assumed

to comprise the transitional bronchiolar compartment. Generations distal to the transitional bronchioles were assumed to comprise the pulmonary region. The surface area of this region was estimated using standard lung models, which compare closely to the values summarized in the U.S. EPA RfC document (U.S. EPA 1994).

Since epithelial thickness in the conducting airways varies as a function of generation in both rodents and humans, average values as summarized in textbooks on pulmonary physiology (Massaro, 1997; Parent, 1992) were used in the model. The epithelial thickness in the transitional airways measured in rats and humans by Mercer et al. (1994) was used in the model

TABLE 3. List of Respiratory Tract-Specific Physiological Parameters Used in the Styrene Model for Mouse, Rat, and Human

Parameter	Symbol	Mouse	Rat	Human	Reference
Tissue thickness (cm)					
UA epithelium	—	0.005	0.005	0.005	(Bogdanffy et al., 1998)
CA epithelium	—	0.0025	0.0025	0.0025	(Parent, 1992)
TA epithelium	—	0.001	0.001	0.001	(Mercer et al., 1994)
PA epithelium	—	0.0003	0.00025	0.0005	(Parent, 1992)
Mucus	—	0.0005	0.001	0.001	Bogdanffy, personal communication
UA submucosa	—	0.01	0.01	0.01	Same
CA submucosa	—	0.005	0.005	0.005	Estimate
TA submucosa	—	0.002	0.002	0.002	Same
Surface area (cm^2)					
UA compartment	SA_x	2.7	13.2	138	(Menache et al., 1997)
CA compartment	SA_x	8.87	48.3	2000	(ICRP, 1994; Oldham et al., 1994; Yeh et al., 1979)
TA compartment	SA_x	0.48	5.5	6220	Same
PA compartment	SA_x	500	3400	540,000	(U.S. EPA, 1994)
Mass transfer coefficient (cm/min)					
UA air-phase	k_a	7200	7200	1980	(Frederick et al., 1998)
CA air-phase	k_a	312	228	181	Estimate[a]
TA air-phase	k_a	1136	481	158	Same
Tissue liquid-phase	k_l	32	16	19.2	Same
Intracompartment clearance (cm^3/min)	K_{ec}	10	40	400	Optimized
Lung microsomal protein (mg/ml)	—	3.8	3.8	3.8	(Mendrala et al., 1993; Pacifici et al., 1988)
Liver microsomal protein (mg/ml)	—	13	11	23	Same
Lung cytosolic protein (mg/ml)	—	68	60	43	Same
Liver cytosolic protein (mg/ml)	—	94	90	45	Same

Note. UA, upper airways; CA, conducting airways; TA, transitional airways; PA, pulmonary airways.
[a]See text for details on estimation of air-phase, liquid-phase, and composite MTC.

TABLE 4. List of Kinetic Parameters Used in the Styrene Model for Mouse, Rat, and Human

Parameter	Symbol	Mouse	Rat	Human	Reference
V_{max} Liver P-450[d]	V_{m1}	200	50–150[g]	50	(Mendrala et al., 1993)
V_{max} UA P-450[d]	V_{m1}	183	98	50	Optimized[a]
V_{max} TA P-450[d]	V_{m1}	362[c]	46.4[c]	1.7[c]	(Hynes et al., 1999; Nakajima et al., 1994)
K_m P-450[e]	K_{m1}	10	10	10	(Csanady et al., 1994; Mendrala et al., 1993)
V_{max} Liver EH[d]	V_{m2}	200	250	900	(Carlson, 1998; Mendrala et al., 1993; Oesch et al., 1983; Schladt et al., 1988)
V_{max} UA EH[d]	V_{m2}	250	250	500	Estimate[b]
V_{max} TA EH[d]	V_{m2}	250	250	500	(Birnbaum & Baird, 1979; Pacifici et al., 1981; Seidegard et al., 1977)
K_m EH	K_{m2}	100	100	100	(Csanady et al., 1994; Mendrala et al., 1993)
V_{max} Liver GST	V_{m3}	11,000	6300	1400	(Griffeth et al., 1987; Mendrala et al., 1993; Pacifici et al., 1981, 1987)
V_{max} UA GST	V_{m3}	1000	1000	300	Estimate[b]
V_{max} TA GST[d]	V_{m3}	1000	1000	300	(Pacifici et al., 1981; Smith et al., 1978)
$K_{m_{GST}}$ GST[e]	K_m	2500	2500	2500	(Csanady et al., 1994)
$K_{m_{SO}}$ GST	K_{m3}	700	700	500	(Hiratsuka et al., 1989; Pacifici et al., 1987)
Liver GSH basal conc.[e]	GSH_B	8300	6300	6000	(Deutschmann & Laib, 1989; Lu, 1999)
UA basal GSH conc.[e]	GSH_B	1000	2500	1000	[Potter, 1995 #5469; estimate]
TA basal GSH conc.[e]	GSH_B	1000	1000	1000	(Cook et al., 1991; Deutschmann & Laib, 1989)
GSH production rate[f]	K_{GSH}	0.012	0.012	0.012	(Potter & Tran, 1993)

Note. UA, upper airways; TA, transitional airways.

[a]Optimized using published value as the initial guess.

[b]Assumed to be equal to Clara-cell values due to insufficient published data.

[c]V_{max} on Clara-cell volume basis in mice, rats and is 461, 141, and 23 nmol/min/ml, respectively.

[d]nmol/min/ml.

[e]nmol/ml.

[f]Per minute.

[g]Shows the parameter range to fit experimental data sets. Mean values are used for dose extrapolation. Mean value for hepatic P-450 V_{max} used in the model for the rat is 93 nmol/min/ml (Mendrala et al., 1993).

and the tissue thickness in the pulmonary region was computed as a ratio of lung weight to surface area. The systemic bronchial circulation, supplying blood to the conducting airways, has been quantified in a number of species and is reviewed in Brown et al. (1997). These values were used in the model for both rodents and humans. Although pulmonary and bronchial circulation both contribute to the blood supply of the transitional bronchioles, it is perfused predominantly by the pulmonary circulation (Butler,

1992). Hence, blood perfusion to this region was estimated as a fraction of the cardiac output, scaled based on the ratio of transitional bronchioles surface area to pulmonary surface area. The remaining venous return from the body was assumed to perfuse the pulmonary region.

The diffusivity of small organic molecules at 37°C in air, based on Chapman-Enskog theory, was estimated to be approximately 6 cm^2/min (Cussler 1999). The air-phase mass transfer coefficient (MTC) in the nasal cavity, which determines the chemical flux from the lumen to the tissue interface, was obtained from Frederick et al. (1998). Under physiologically normal breathing conditions the flow is laminar in the conducting and transitional airways (Chang & Paiva, 1989). Theoretical formulation for the convective MTC under laminar flow conditions in a circular pipe has been derived and is shown to be a function of flow rate, air-phase diffusivity, and the pipe dimensions* (Cussler, 1999). Based on this theoretical formulation, the air-phase MTC was estimated in rodents and humans for each generation in the conducting airways and an averaged values used for this compartment. The gas-phase MTC in the transitional airway in the rodent was computed based on airway dimension in the 16th generation, and in human was computed based on airway dimension in the 18th generation. The air-phase MTC was assumed to be the same for ST and SO in all the respiratory tract compartments. The liquid-phase MTC, which determines the chemical flux from the interface into the tissue, was estimated as a ratio of liquid-phase chemical diffusivity by half the mucus thickness (i.e., diffusion length). The composite air-to-tissue MTC, which determines the net chemical flux from the lumen into the tissue, was calculated as a function of the air-phase MTC, liquid-phase MTC, and the corresponding tissue:air partition coefficient (U.S. EPA, 1994). The liquid-phase diffusivity of ST and SO was estimated to be 0.0002 cm^2/min, approximately equal to the diffusivity of benzene in water (Cussler, 1999).

Model Parameterization of Kinetic Constants

P-450 Activity The kinetic constants (V_{max}, K_m) for hepatic P-450 activity toward ST have been reported by Mendrala et al. (1993) in B6C3F1 mice, F344 rats, and human liver tissue microsomal fraction (Table 4). The V_{max} values were reported on a per milligram microsomal protein basis. For its use in the model, the liver P-450 activity was converted to a per milligram tissue basis based on the amount of microsomal protein per milligram liver tissue (Mendrala, personal communication) (Table 4). These results showed that the affinity of hepatic P-450 was similar in all three species, and the capacity to form SO from ST was greatest in mice and lowest in humans, on a per gram tissue basis (Table 4).

Metabolic constants for pulmonary cytochrome P-450 activity toward ST are available from two principle sources, in vitro measurements using micro-

*MTC = 1.62 $(D^2v/Ld)^{1/3}$ where D is the air-phase diffusivity in cm^2/min, v is the average fluid velocity in cm/min, L is the airway length, and d is the airway diameter.

somal protein from whole lung, or whole-cell preparations enriched for Clara cells or Type II cells. Hynes et al. (1999) measured *R*-SO and *S*-SO production in isolated enriched fractions of mouse and rat Clara cells and Type II cells and presented the activity on a million cell basis. For its use in the model, the total P-450 activity was first obtained by combining the activity for the *R* and the *S* form. This total P-450 activity on a million Clara cell basis was then converted to activity per milliliter Clara cell basis using information on the Clara-cell volume in rodent lungs (Mercer et al., 1994). Using the ratio of the Clara-cell volume to the total epithelial cell volume in the terminal bronchioles as a correction factor, pulmonary P-450 activity on a milligram bronchioles tissue basis was computed in rodents (Appendix). The resulting P-450 activity (V_{max}) of 362 nmol/min/ml tissue and 46.4 nmol/min/ml tissue in the terminal bronchioles in mice and rats, respectively, is within a factor of 2 of hepatic P-450 activity in the respective species.

Nakajima et al. (1994) reported lung P-450s activity in humans by determining the rate of formation of styrene glycol from ST in human lung microsomes using tissue samples from nonsmokers (Table 4). Their activity, reported on a per milligram microsomal protein basis, was converted to a per milligram lung tissue basis after accounting for milligram protein per milligram lung tissue in humans (Pacifici et al., 1988). Since P-450 activity in the lung is limited to Clara cells (Hynes et al., 1999), which form a small fraction of the lung volume, expressing the P-450 activity on a per milligram whole lung tissue basis will dilute the Clara-cell-specific metabolism, and is thus an inappropriate measure of the regional P-450 activity in the Clara-cell-rich compartment of the lung. Consistent with our MOA, the primary focus of this modeling effort was to characterize the concentration of ST and SO in the transitional bronchioles (i.e., the Clara-cell-rich region that forms the target site in mice for ST-induced toxicity). Approximately 85% of the total Clara cells in the lung are present in the transitional bronchioles in humans (Parent, 1992). Hence, to construct the parameterization for the transitional bronchiolar region based on the total lung activity the following procedure was adopted (Appendix). First, the P-450 activity on a per milligram lung tissue basis was corrected by the ratio of the lung volume to the Clara cell volume, to reflect the activity in the relevant cell type. Subsequently, the ratio of the Clara cell volume in the transitional bronchioles to the total epithelial cell volume in the transitional bronchioles was used as the correction factor to obtain the pulmonary P-450 activity on a milligram bronchioles tissue basis, resulting in a P-450 activity of 1.7 nmol/min/ml tissue.

Epoxide Hydrolase The kinetic constants (V_{max}, K_m) for hepatic EH activity toward SO have been reported by Mendrala et al. (1993) in B6C3F1 mice, F344 rats, and human liver tissue samples on a per milligram microsomal protein basis. This activity was converted to a milligram whole liver tissue basis after correcting for the amount of microsomal protein per milligram whole liver tissue (Table 4). Various other studies have also mea-

sured EH activity using liver microsomal fraction in mice (Carlson, 1998), rat (Griffeth et al., 1987; Oesch et al., 1983; Seidegard et al., 1977), and human (Schladt et al., 1988). These studies show that the EH activity is approximately fourfold higher in humans compared to rodents, while the affinity is comparable in all three species.

Pulmonary EH activity toward SO has also been demonstrated in microsomal fractions from rat (Oesch et al., 1983; Seidegard et al., 1977; Smith et al., 1978), mouse, and human lung tissue (Birnbaum & Baird, 1979; Pacifici et al., 1981). Similar to pulmonary P-450 activity, EH activity is also present in only specific cell types such as the Clara cells, bronchial epithelial cells, and alveolar Type II cells (Baron & Voigt, 1990). Since these cell types form only a small fraction of the lung volume, EH activity expressed on a per milligram whole lung tissue basis needs to be corrected to reflect the activity in the relevant cell types. Volume of Type II cells is 10- to 100-fold higher than Clara cells or bronchial epithelial cells in both rodents and humans (Stone et al., 1992). Hence, EH activity on a per milligram lung tissue basis was first corrected based on the ratio of the lung volume to the Type II cell volume, to estimate EH activity in Type II cells.

Immunohistochemical staining data in rats (Baron & Voigt, 1990; Jones et al., 1983) show EH activity in the Clara cells is approximately three times that in the alveolar Type II cells. Assuming a similar relationship in mouse and human, Clara-cell EH activity was set to three times the EH activity in Type II cells and EH activity in the transitional airway compartment obtained based on the fractional Clara-cell volume. The resulting EH activity (V_{max}) on a milligram bronchiole tissue basis was comparable to hepatic EH activity, and the human pulmonary EH activity was approximately twice that of rodents. The pulmonary EH affinity (K_m) in rats was estimated to be 0.25 m*M*, comparable to rat hepatic EH affinity (Seidegard et al., 1977). Since independent measures of pulmonary EH affinity in mice and humans were not available, EH affinity in mouse and human was assumed to be similar to rat in the model because hepatic EH affinity is similar across the three species (Mendrala et al., 1993; Pacifici et al., 1988).

Glutathione-*S*-Transferase The GSTs are a family of enzymes that catalyze the conjugation of SO with GSH. The GST-catalyzed reaction between GSH and SO is typically described using a two-substrate (ping-pong) model, characterized by three kinetic constants: maximum reaction velocity (V_{max}), GST affinity for GSH (K_{mGSH}), and GST affinity for SO (K_{mSO}). Mendrala et al. (1993) measured hepatic GST activity and affinity toward SO in B6C3F1 mice, F344 rats, and human liver tissue samples by incubating ^{14}C-SO with cytosolic protein in an excess of GSH (10 m*M*). They reported a GST V_{max} on a per milligram cytosolic protein basis, which was converted to a per milligram tissue basis based on the amount of cytosolic protein per milligram liver tissue (Mendrala, personal communication). Pacifici et al. (1987) studied detoxication of SO by human liver cytosolic fraction and have characterized GST activity and affinity toward GSH by varying the concentration

of GSH (0.5–25 m*M*) and keeping the concentration of SO relatively high (6 m*M*).

Pacifici et al. (1981) measured cytosolic GST activity using human, rat, and mouse lung samples and observed the activity in humans to be twice that of mice and rats (Table 4). They reported GST activity on a per milligram cytosolic protein basis, which was converted to a per milligram tissue basis based on the amount of cytosolic protein per milligram lung tissue. Comparable GST activity is found in most lung cell types in all three species (Anttila et al., 1993; Coursin et al., 1992; Mace et al., 1998). Hence the GST activity in the terminal bronchiole compartment was assumed to be the same as the measured GST activity in the whole lung. A summary of P-450, EH, and GST activity in the liver and lung in all three species is provided in Table 4.

Glutathione Hepatic and pulmonary GSH levels in rats and mice have been measured in various studies (Deutschmann & Laib, 1989; Potter & Tran, 1993) and are summarized in Table 4 based on average values from these individual studies. Based on the published data, intracellular GSH in the lung is approximately one-sixth of that in the liver, on a unit mass basis. Measurements show a similar relationship for GSH content between human liver and lung tissue (Cook et al., 1991; Lu, 1999). The apparent first-order rate constant for GSH turnover was estimated in different rat tissues, including the liver and the lung, by monitoring the decrease in GSH specific activity following an iv injection of [^{35}S]cysteine (Potter & Tran, 1993). A rate constant of 0.142/h and 0.011/h was estimated for the liver and the lung tissue, respectively. Although similar measurements are not available in mouse and humans, this physiological constant is predicted to be comparable across species (D'Souza et al., 1988).

Stereospecific Metabolism of ST and SO

Species differences in the stereospecific metabolism of ST to *R*-SO and *S*-SO have been demonstrated in both the liver and the lung of rats and mice (Hynes et al., 1999). The *R*-enantiomer is preferentially formed in the mice, with a *R:S* ratio of 1.18 in the liver microsomes and 2.4 in the lung microsomes (Table 5). In the rat, more *S*-SO was formed than *R*-SO in both the liver and lung, with a *R:S* ratio of 0.57 in the liver and 0.52 in the lung (Table 5). Similar studies using human lung and liver tissue are quite limited. Carlson showed that 7 human liver samples produced *R:S* ratios less than 1, while this ratio was near 1 in 1 of 7 human lung samples that metabolized ST enough to detect SO. No metabolism of styrene to SO was detected in the other six samples.

EH activity toward SO is also stereospecific, favoring the more reactive *R*-enantiomer over the *S*-enantiomer in both the lung and liver of mice (Carlson, 1998; Carlson et al., 1998; Linhart et al., 2000). A kinetic study of EH reaction in rat liver microsomes showed a marked difference in affinity and activity of EH between *S*-SO and *R*-SO, with a K_m of 0.155 m*M* and a V_{max} of 44.1 nmol/mg protein/min for the *S*-SO and a K_m of 0.029 m*M* and

TABLE 5a. Stereospecific Kinetic Parameters for ST and SO Metabolism in Rodents

Parameter	Mouse		Rat		Reference
	R	*S*	*R*	*S*	
V_{max} P-450 Liver[a]	108.3	91.7	33.8	59.2	(Hynes et al., 1999)
V_{max} P-450 t. bronchioles[a]	211.8	88.2	130	250	(Hynes et al., 1999)
K_m P-450[b]	10	10	10	10	(Csanady et al., 1994)
V_{max} EH liver[a]	66.7	133.3	570	151	(Carlson, 1998; Watabe et al., 1983)
V_{max} EH t. bronchioles[a]	125	125	200	50	(Carlson 1998)
K_m EH[b]	29	155	29	155	(Watabe et al., 1983)
V_{max} GST liver[a]	4400	6600	2400	3600	(Hiratsuka et al., 1989)
V_{max} GST t. bronchioles[a]	400	600	400	600	Estimate
K_{mSO} GST[b]	700	2000	700	2000	(Hiratsuka et al., 1989)
K_{mGSH} GST[b]	2500	2500	2500	2500	(Csanady et al., 1994)

[a]nmol/min/ml.
[b]nmol/ml.

V_{max} of 11.6 nmol/mg protein/min for the *R*-SO (Watabe et al., 1983) (Table 5). Thus, at concentrations below both K_ms, *S*-SO may be expected to be hydrolyzed 1.4 times faster than the *R*-SO, if metabolism is formulated separately for *R*- and *S*-SO. However, in a racemic mixture of SO, *R*-SO, with a smaller K_m, may inhibit the enzymatic hydrolysis of *S*-SO, resulting in larger clearance of *R*-SO. Preliminary analysis implementing EH metabolism as competitive inhibition of *S*-SO hydrolysis by *R*-SO in the model had insignificant (<1%) effect on steady-state target tissue SO concentrations. When hepatic and pulmonary microsomal preparations from CD-1 mice were compared for their ability to metabolize racemic SO, *R*-styrene glycol formation was favored over *S*-styrene glycol by a ratio of 2.6 in the liver and a ratio of 5.6 in the lung (Carlson, 1998). The hydrolysis of SO proceeded in an enantiospecific manner when human liver microsomal preparations were

TABLE 5b. Steady-State Concentrations of *R*-SO and *S*-SO in the Terminal Bronchioles in Mice and Rats for Exposure Concentrations Used in the Respective Rodent Chronic Bioassays

Mouse Exposure (ppm)	*R*-SO (nmol/ml)	*S*-SO (nmol/ml)	*R*/*S* Ratio
20	4.3	1.5	2.87
40	5.3	2.0	2.65
80	6.2	2.5	2.48
160	7.2	3.3	2.2
Rat Exposure (ppm)	***R*-SO (nmol/ml)**	***S*-SO (nmol/ml)**	***R*/*S* Ratio**
50	0.65	0.93	0.7
200	1.6	2.2	0.73
500	1.98	2.7	0.73
1000	2.0	2.75	0.73

incubated with *R*-SO and *S*-SO separately, with *S*-SO having approximately six times higher K_m and five times higher V_{max} than *R*-SO (Wenker et al., 2000).

A kinetic study to quantify GSH conjugation of SO enantiomers by GST in SD rat liver cytosol also showed stereospecificity, favoring clearance of the *R*-SO compared to *S*-SO (Hiratsuka et al., 1989). The apparent V_{max} and K_m for rat hepatic GSH conjugation with *R*-SO is 66.7 nmol/mg protein/min and 0.7 m*M*, while the corresponding values for *S*-SO is 100 nmol/mg protein/min and 2 m*M* (Hiratsuka et al., 1989) (Table 5). The stereoselectivity of GSH conjugation in the mouse has not been determined and has been assumed to be similar to rats in the current PBPK model.

RESULTS

Model Validation

Ten independent data sets, ranging from closed-chamber data to concentration measurements of ST and SO in multiple tissues following multiple routes of exposure, were used to validate various dose metrics in the mouse, rat, and human. The results of these modeling efforts are described next to illustrate the extent and success of the validation of model-predicted concentrations of ST and SO in the blood and other tissues. This multi-data-set validation was conducted using the average values for the physiological and kinetic parameters presented in Tables 2–4, with only minimal modification to a few metabolic and flow parameters on a case-by-case basis (as noted in the figure legends).

Delivered dose to the lower airways and available dose for systemic extraction require accurate characterization of the extraction of inhaled vapors in the nasal cavity (Barton et al., 2000). Morris and coworkers measured extraction of ST in surgically isolated upper respiratory tract of anesthetized CD mice and SD rats at multiple flow rates and concentrations to examine the effect of flow rate and concentration on nasal extraction (Morris, 2000). These data sets on nasal extraction of ST in both rats and mice were used to validate the nasal cavity portion of the respiratory tract model. The model accurately predicted the experimentally observed nonlinear behavior in nasal extraction as a function of flow rate and concentration in both rodent species, with extraction decreasing with increases in flow rate and concentration (Figure 3). Model fit to the nasal extraction data is a validation of metabolism and flow parameters in rat and mouse upper airway compartment.

Closed-chamber experimental data (Filser et al., 1993) came from exposing 2 SD rats for 12 h to 780–3800 ppm ST or 5 B6C3F1 mice for 10 h to 550–5000 ppm ST (Csanady et al., 1994; Ramsey & Andersen, 1984). The rat and mouse PBPK models were used to simulate this data set. Model simulated chamber concentrations closely matched the measured chamber concentration time course (Figure 4). Liver metabolic capacity was reduced by 40% of the measured in vitro value to fit the rat closed-chamber data. In contrast, alveolar ventilation rates were reduced by 30%

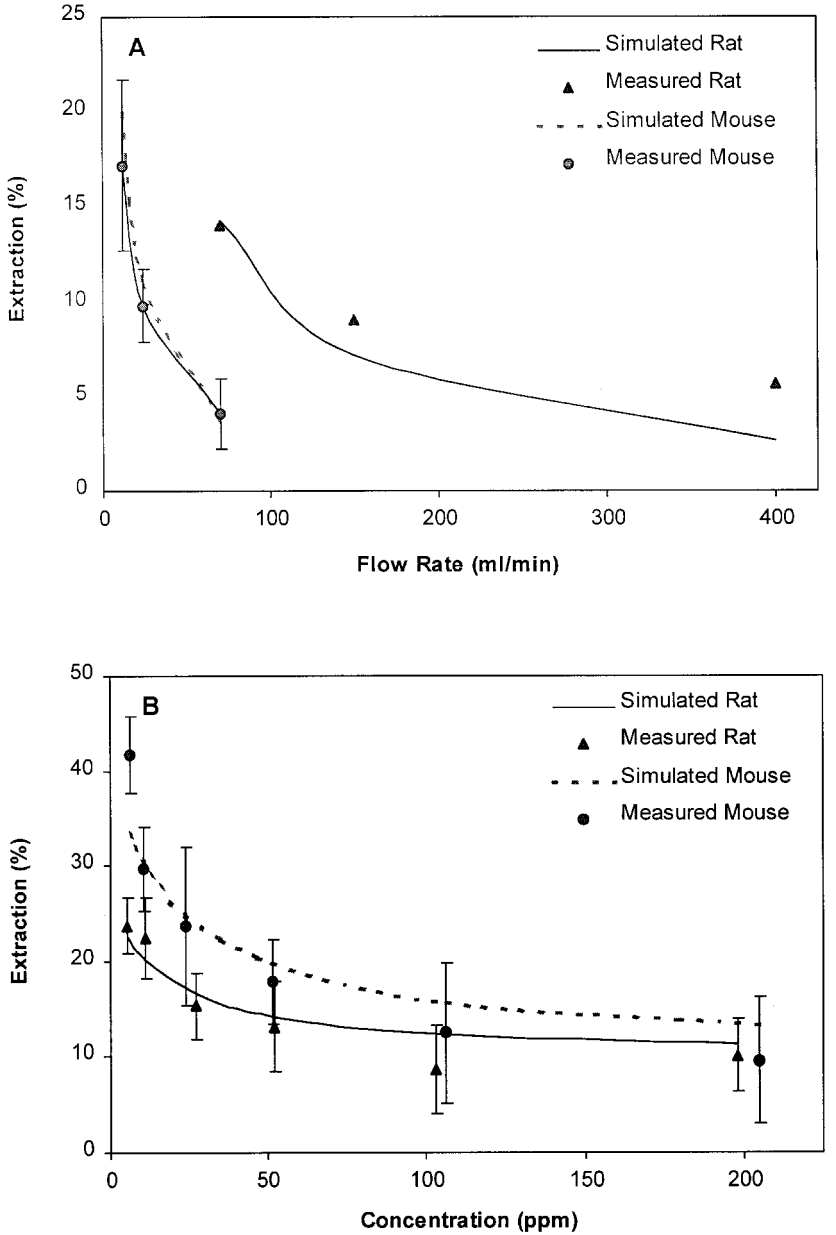

FIGURE 3. Upper respiratory tract extraction of styrene in mice and rats as a function of (A) flow rate and (B) inhaled ST concentration (Morris et al., 2000). The error bars on the data points represent standard deviations.

cally normal value to fit the mouse closed-chamber data. Mendrala et al. (1993) report a wide range for in vitro measurements of hepatic P-450 activity in rats (7.9 ± 2.4 nmol/min/mg protein in SD rats and 14 ± 8.6 nmol/min/mg protein in F344 rats). Reductions in ventilation rates have been observed in closed-chamber experiments (Johanson & Filser

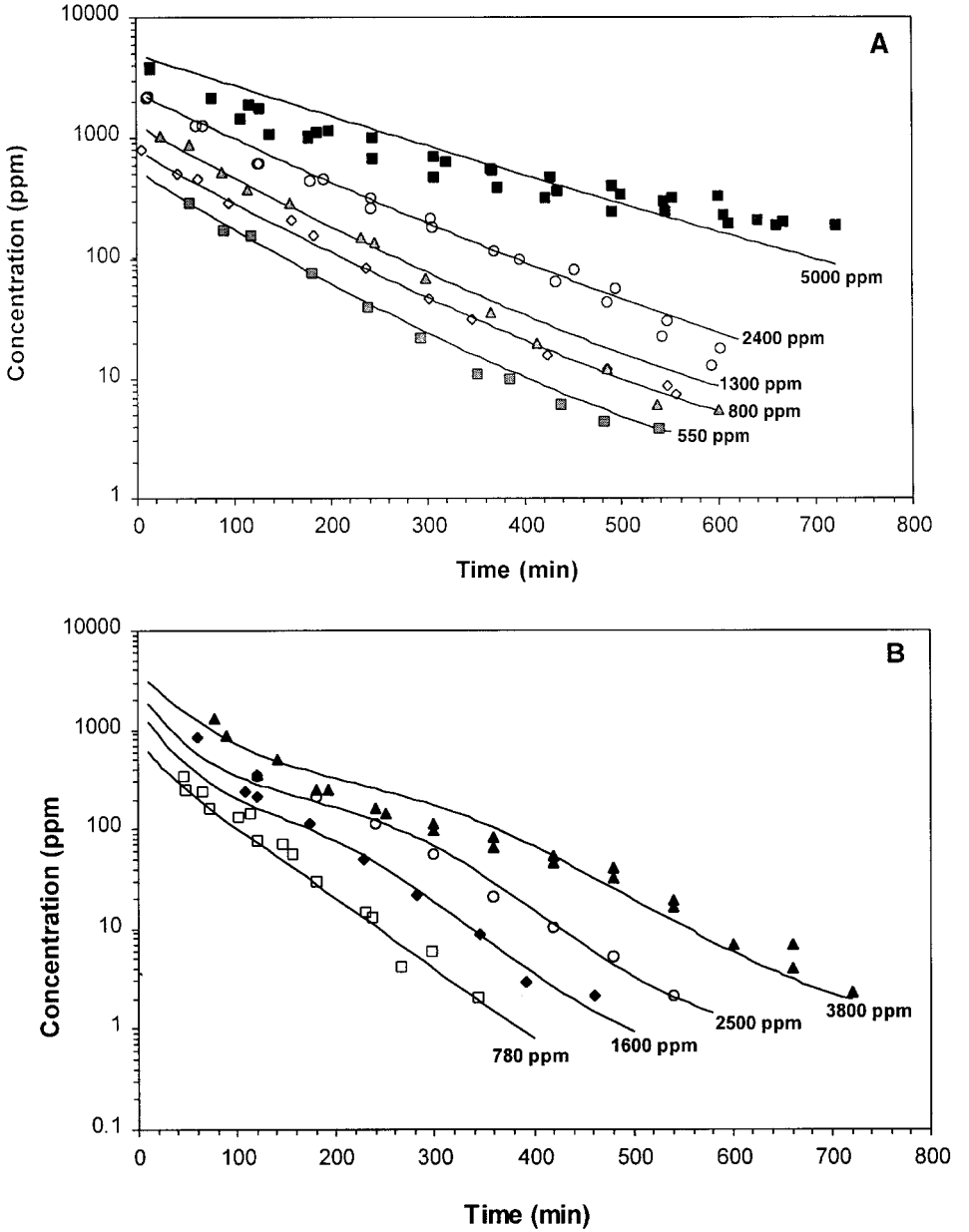

FIGURE 4. Model fit to closed chamber inhalation data set exposing (A) 5 mice or (B) 2 rats for 12 h to a wide range of ST concentrations (Filser et al., 1993). Average model parameters presented in Tables 2–4 provide adequate fit to data. However, to obtain optimal model fit to data the mouse model, simulations were conducted using an alveolar ventilation of 13 ml/min and a hepatic blood flow rate equal to 30% of cardiac output. Similarly, rat model simulations were conducted using a hepatic P-450 activity of 50 nmol/min/ml tissue and a hepatic blood flow rate equal to 15% of cardiac output. Brown et al. (1997) report a wide range for alveolar ventilation rate and total hepatic blood perfusion rate in rodents. The remaining model parameters are as presented in Tables 2–4.

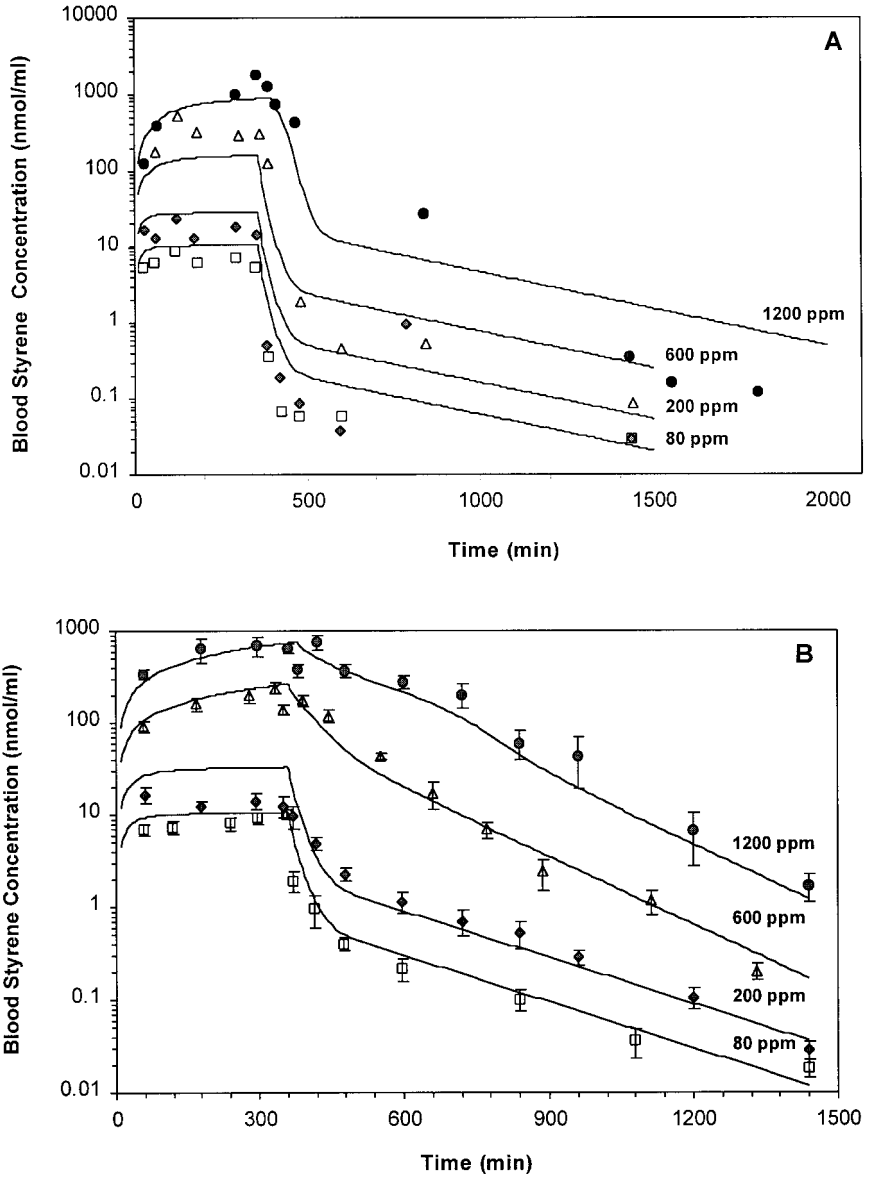

FIGURE 5. Model fit to blood ST concentration time course in (A) mice and (B) rats, following 6 h of inhalation exposure to a wide range of ST concentration (Ramsey & Young, 1978). Average model parameters presented in Tables 2–4 provide adequate fit to data. However, to obtain the optimal model fit to data, shown here, the mouse model simulations were conducted using an alveolar ventilation rate of 12 ml/min and fat and liver blood flow rates of 1% and 30% of cardiac output, respectively. Similarly, rat model simulations were conducted using an alveolar ventilation rate of 75 ml/min and fat and liver blood flow rates of 2% and 30% of cardiac output, respectively. The alveolar ventilation rates used for these simulations are identical to the values used by Ramsey and Andersen (1984) to fit the same dataset. The remaining model parameters are as presented in Tables 2–4. The error bars on the data points represent standard deviations.

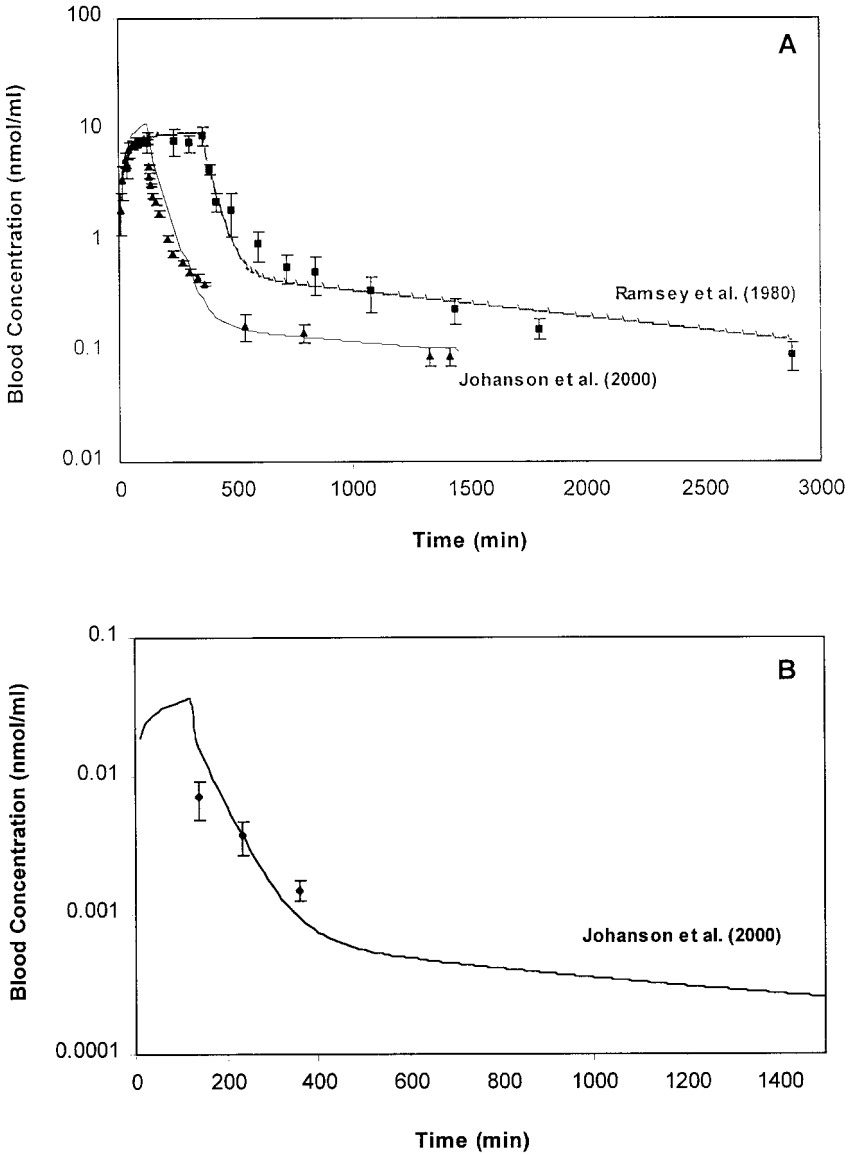

FIGURE 6. Model fit to blood (A) ST and (B) SO concentrations in human volunteers following a 6-h inhalation exposure to 80 ppm ST (Ramsey & Young, 1978) and a 2-h inhalation exposure to 50 ppm ST (Johanson et al., 2000). Model simulations were conducted using the experimentally measured ventilation rates and in vitro measures of hepatic enzyme activity in humans. The remaining model parameters are as presented in Tables 2–4. The error bars on the data points represent standard deviations.

been applied in PK models to fit the closed-chamber data in previous studies (Johanson & Filser, 1993). Since concentration changes from closed-chamber experiments are a reflection of systemic clearance in the experimental animals, model fit to the closed chamber data is a validation of systemic metabolism parameters in rats and mice.

Ramsey and Young (1978) measured blood ST concentration time course in rats and mice following a 6-h inhalation exposure to a wide range of ST concentrations (80–1200 ppm). A gradual increase in the ST blood concentration during exposure, followed by a biphasic drop in the venous concentration postexposure, was observed (Ramsey & Young, 1978). The PBPK model was validated against this data set. Using in vitro measures of hepatic enzyme activity and an alveolar ventilation rate 30% lower than the physiologically normal values, the rodent PBPK model predictions matched the measured blood concentration data in both rats and mice (Figure 5). Brown et al. (1997) report a wide range for alveolar ventilation rates in rats (63–275 ml/min) and mice (16–29 ml/min). Ramsey and Young (1978) also measured blood ST concentration time course in human volunteers following a 6-h exposure to 80 ppm ST. More recently, Johanson and coworkers measured the human blood concentration of ST and SO following a 2-h exposure to 50 ppm ST under light activity, while simultaneously measuring the minute ventilation in all the human volunteers (Johanson et al., 2000). Using these experimentally measured ventilation rates and in vitro measures of hepatic enzyme activity in humans, the PBPK model simulations of blood ST and SO were in close agreement with measured values in humans (Figure 6). Model fit to the blood concentration data is a validation of systemic metabolism and flow parameters in rodents and humans.

During a chronic inhalation bioassay, Cruzan and coworkers analyzed levels of ST and SO in the blood of rats and mice immediately after a 6-h inhalation exposure (Cruzan et al., 1998, 2001). The measurements were conducted on rodents from the 5 dose groups used in the chronic study during wk 95 in rats and wk 74 in mice. The blood concentration of SO tended toward saturation at the highest exposure in rats, whereas the blood SO concentration increased in proportion to ST exposure concentration in mice with no evidence of saturation of metabolism. The PBPK model simulations were able to reproduce these results without altering model parameters (Figure 7), except for the measured increased body weight and fractional fat volume. Model fit to this data set is a validation of the systemic phase I and II metabolism parameters in rodents used in the inhalation chronic bioassay.

Pharmacokinetic studies measuring ST and SO exposure–dose relationships in the liver and the lung tissue provide useful data for direct validation of model predicted tissue concentrations. Withey and Collins (1979) collected exposure–concentration data in blood, liver, and lung tissue immediately following a 5-h inhalation exposure to ST at multiple concentrations (50–2000 ppm) in Wistar rats. The distribution pattern of ST is dose dependent, but the liver consistently has a higher concentration than the lung (Withey & Collins, 1979). The model provides a good fit to the exposure–dose data for all three tissues without altering any of the measured tissue metabolism or partition coefficient parameters (Figure 8).

Löf et al. (1984) studied the concentration time-course and exposure–dose relationship for ST and SO in mouse tissues after intraperitoneal administration of ^{14}C-ST. They measured the blood ST and SO concentration time course following an ip dose of 3.8 mmol/kg ^{14}C-ST in mice. After estimating

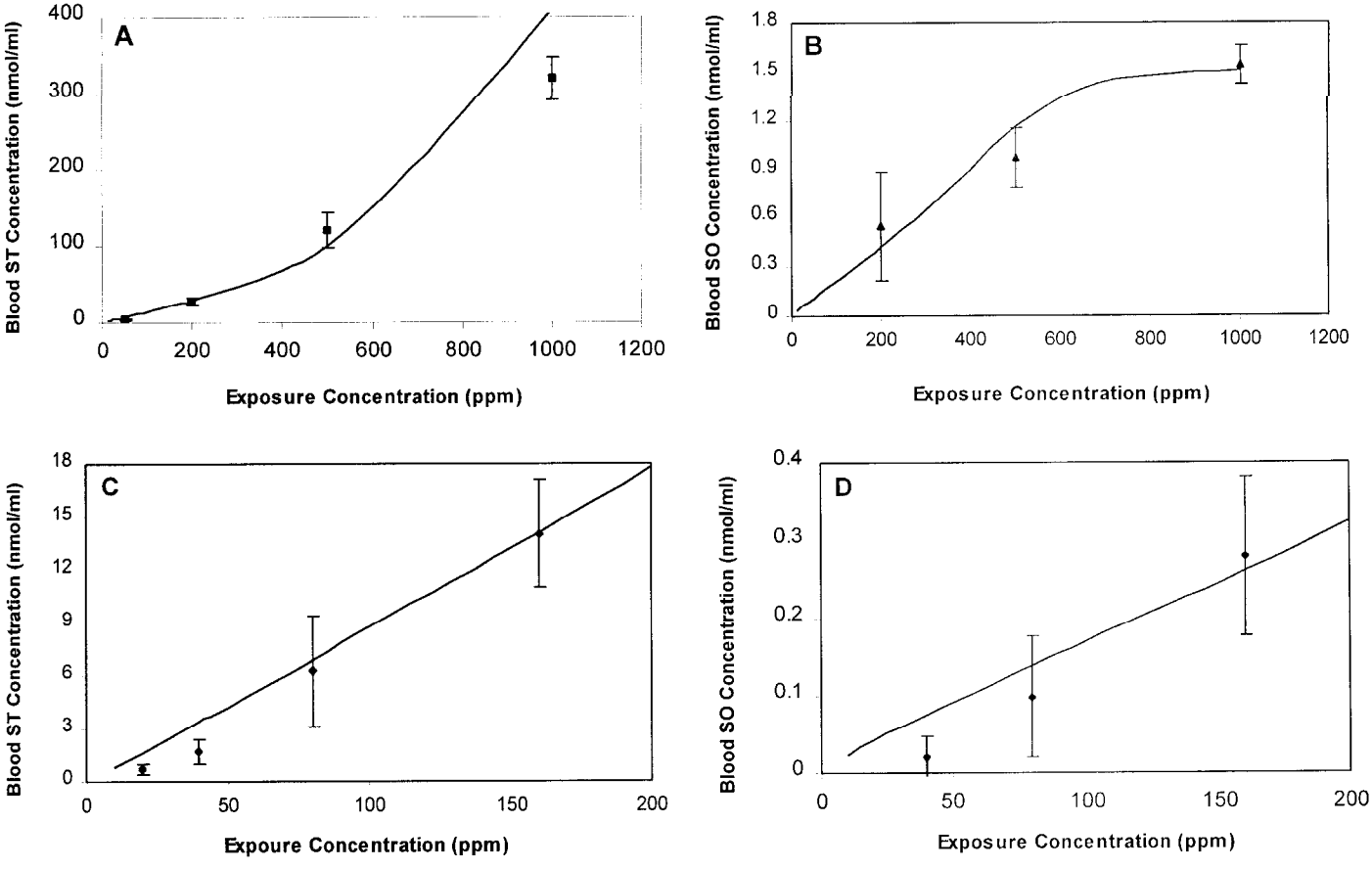

FIGURE 7. Model fit to blood concentration of (A) ST in rat, (B) SO in rat, (C) ST in mouse, and (D) SO in mouse, measured immediately after a 6-h inhalation exposure to ST. These measurements were made during wk 95 in a chronic inhalation bioassay in rats and during wk 74 in mice (Cruzan et al., 1998, 1999). Model simulations were conducted using measured body weights of 42 g in mice and 725 g in rat and an estimated fat volume of 20% of body weight in both rodent species. The remaining model parameters are as presented in Tables 2–4. The error bars on the data points represent standard deviations.

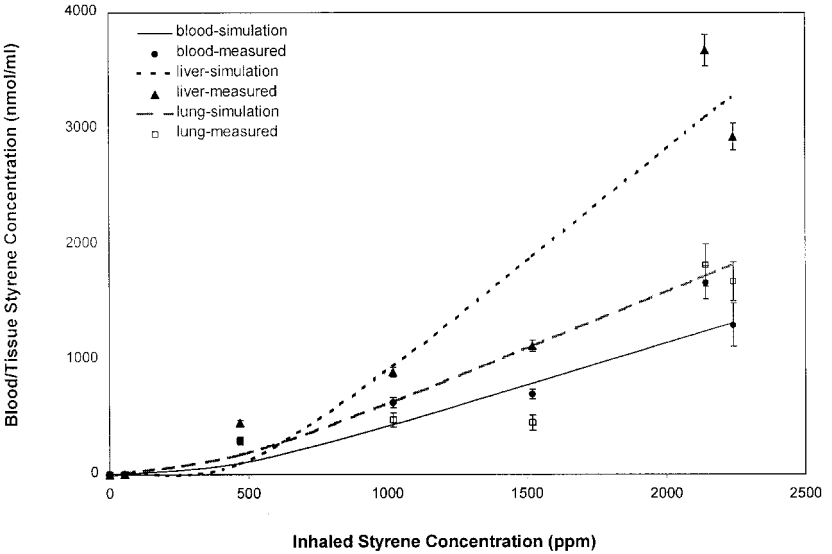

FIGURE 8. Model fit to blood, liver, and lung ST concentration in rats immediately after a 5-h inhalation exposure to a wide range of ST concentrations (Withey & Collins, 1979). To obtain optimal model fit to data, the rat model simulations were conducted using a hepatic P-450 activity of 150 nmol/min/ml tissue. The remaining model parameters are as presented in Tables 2–4. The error bars on the data points represent standard deviations.

the first-order uptake rate into the liver using the ST concentration time-course data, the model was able to simulate the blood SO concentration time course (Figure 9). The jump in the measured blood SO concentration, resulting from depletion of hepatic GSH, is captured in model predictions. Significant dose-related reduction in hepatic GSH has been observed in mice following inhalation exposure to styrene (Morgan et al., 1993). Löf et al. (1984) also analyzed blood and tissue samples from the liver and the whole lung for ST and SO in mice, 2 h after ip dose of 1.1, 2.3, 3.4, and 5.1 mmol/kg ^{14}C-ST, and determined the exposure–dose relationship for ST and SO in the liver and lung tissues (Lof et al., 1984). The PBPK model simulations predict a similar trend and provide a good fit to the data (Figure 10). The model predictions for ST and SO concentration in the whole lung are based on an average value from the three lower lung compartments, weighted according to the respective volumes. A lack of experimentally measured tissue concentrations of ST and its metabolic products in the mouse transitional bronchioles (presumed site of origin for the mice lung tumors) prevents direct validation of the model predicted target tissue concentrations of the active moiety. All these data sets taken together provide a robust validation of the PBPK model across species and at multiple target sites, including the whole lung but not the terminal bronchioles, for both ST and SO, and thus provide a high level of confidence in the model predicted tissue concentrations at these sites.

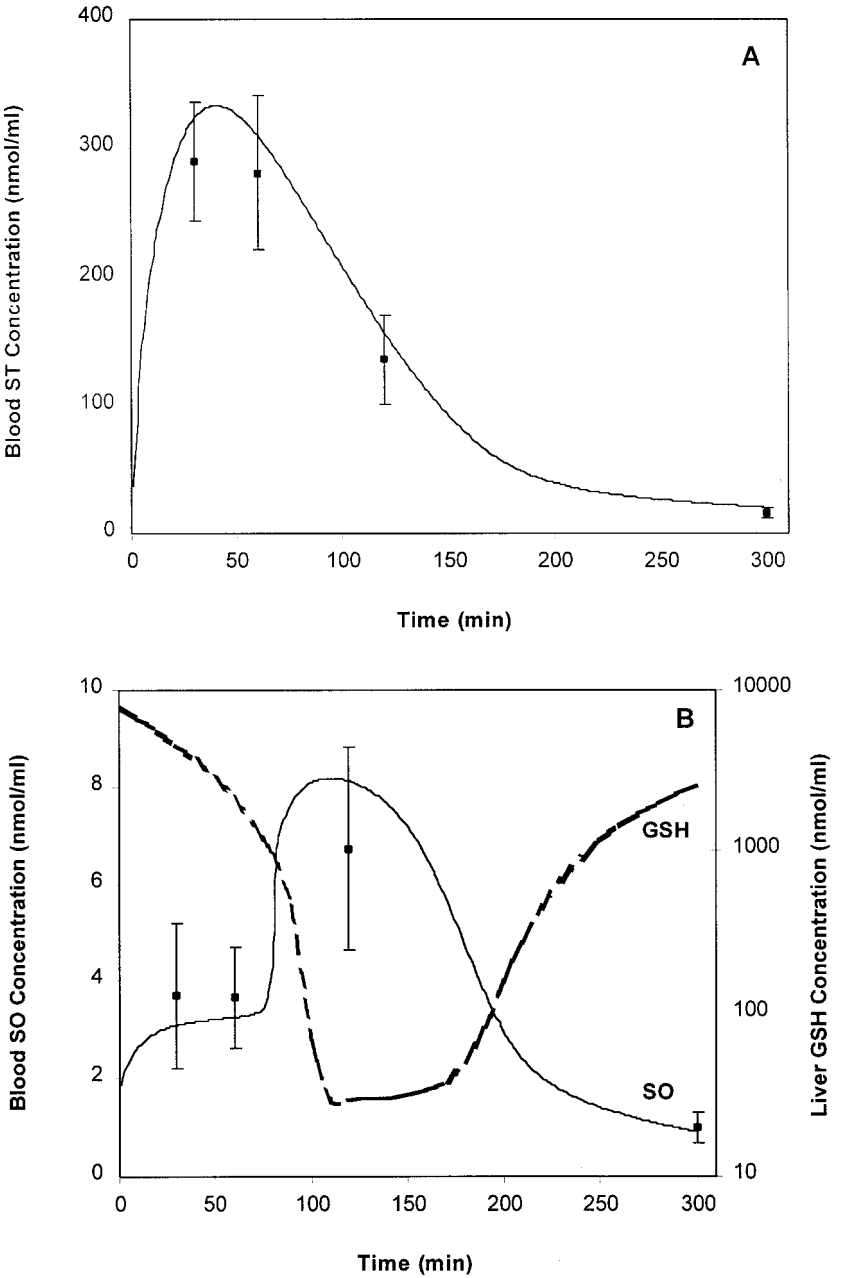

FIGURE 9. Model fit to (A) blood ST and (B) blood SO and hepatic GSH concentration time course in mice following an intraperitoneal administration of 3.8 mmol/kg ^{14}C-ST (Löf et al., 1984). Model-derived ST blood concentration-time profile was visually fit to measured data by adjusting K_{ip} (first-order uptake rate from the intraperitoneal cavity ~0.011/min), and the model simulation for SO blood concentration profile was conducted using the same K_{ip} value. The remaining model parameters are as presented in Tables 2–4. The error bars on the data points represent standard deviations.

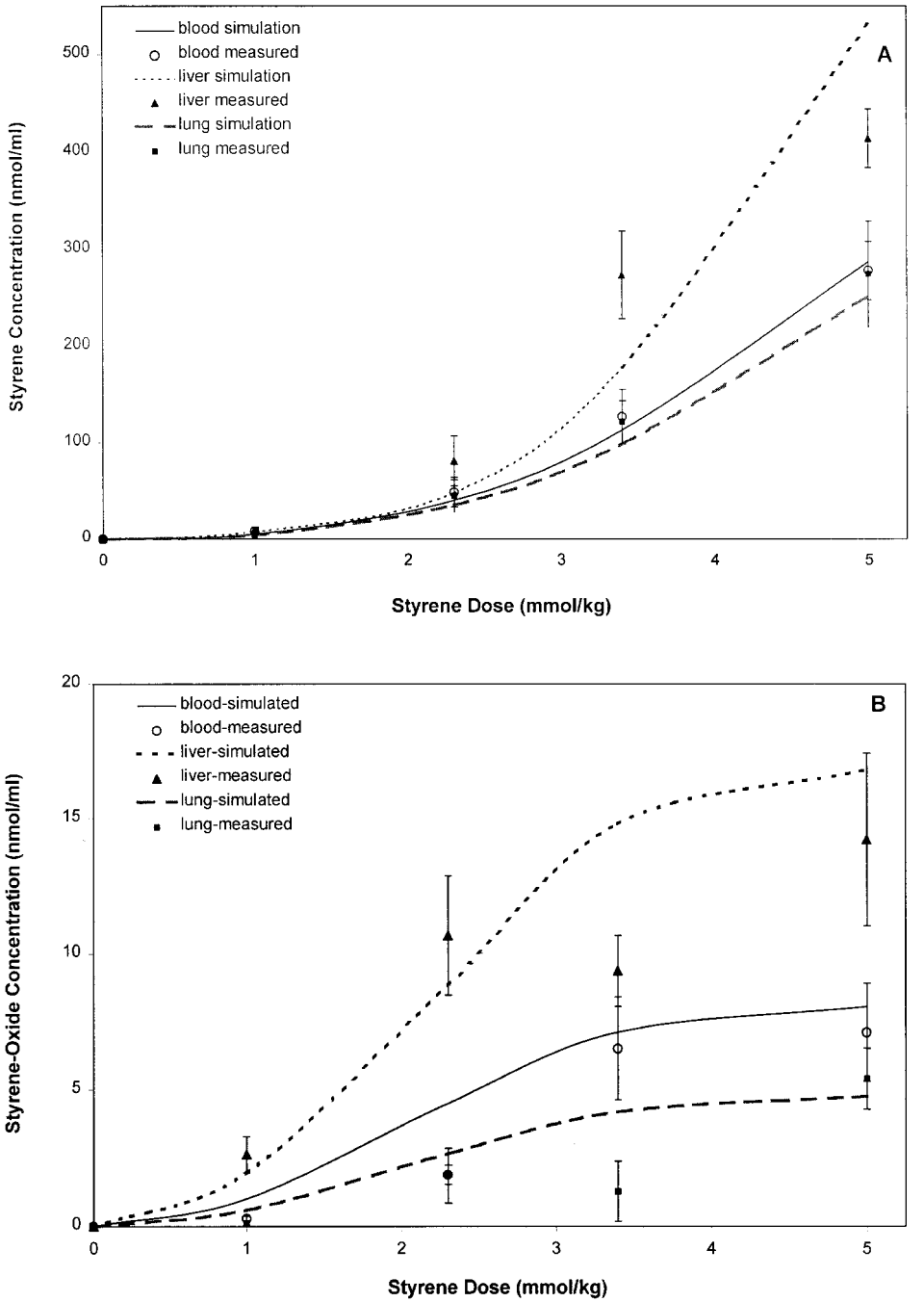

FIGURE 10. Model fit to blood, liver, and lung (A) ST and (B) SO concentrations in mice 2 h after intraperitoneal administration of various doses intraperitoneally administered ST (Löf et al., 1984). Model simulations conducted assuming a first order uptake rate (K_{ip}) of 0.011/min. The error bars on the data points represent standard deviations.

Evaluation of Internal Dose Metrics

PBPK model-based quantitative dose-response assessments are usually conducted using an internal (i.e., tissue level) dose metric that has a direct mechanistic link to the response. If information on target tissue concentrations of the putative toxicant is lacking, systemic blood concentrations are often used as a surrogate dose metric under the assumption that tissue concentrations correlate with blood concentrations. However, exposure–dose relationships for inhaled metabolized vapors are different between the portal of entry tissues and systemic tissues. The PBPK model was used to simulate steady-state SO concentrations in arterial blood and the terminal bronchioles in mice to discern if the tissue concentrations of SO correlate better with both the tumor response and precursor events compared to systemic blood concentrations. Because adenomas are considered precursors to the observed carcinomas, the benign and malignant neoplasms in males, the most sensitive sex, were combined to give the total neoplastic response and compared to SO concentration in the terminal bronchioles and in the systemic blood (Figure 11). Similarly, the incidence of bronchioloalveolar focal hyperplasia (preneoplastic event) in male mice was combined with the neoplastic response to give the total incidence of precursor lesions and compared to SO concentration in the terminal bronchioles and in the systemic blood (Figure 11). Visual inspection of Figure 11 suggests that the trend in the percent increased incidence of total neoplastic lesions and precursor response is better correlated to predicted SO concentration in the terminal bronchioles, which tends toward a saturation with exposure, rather than the systemic (as measured by blood) SO concentrations, which increase linearly with exposure. The correlation coefficient for the transitional bronchiolar tissue SO concentrations with the neoplstic response (.89) and precursor response (.99) are higher than the correlation coefficient for blood SO concentrations with the neoplastic lesions (.78) and precursor response (.70). This suggests that the target tissue SO concentration in the terminal bronchioles maybe a more appropriate dose metric for conducting dose-response assessment than systemic blood SO concentration.

Interspecies Tissue Dose Comparison

A comparison of the exposure–dose relationship for SO in the transitional bronchioles (target tissue) in mouse (sensitive species), rats, and human (target species) was conducted using the ST PBPK model. Given the uncertainty in the cell of origin for the tumors, region-specific dose was considered the most appropriate metric for making these comparisons. This dose metric is expected to be representative of the average SO concentration in the tissue volume that is populated by Clara cells and other neighboring cell types (including Type II cells that could be in close proximity to Clara cells at the distal end of the terminal bronchioles). Figure 12 shows model-simulated steady-state SO concentrations in the transitional bronchioles in the mouse, rat, and human at the end of a continuous exposure.

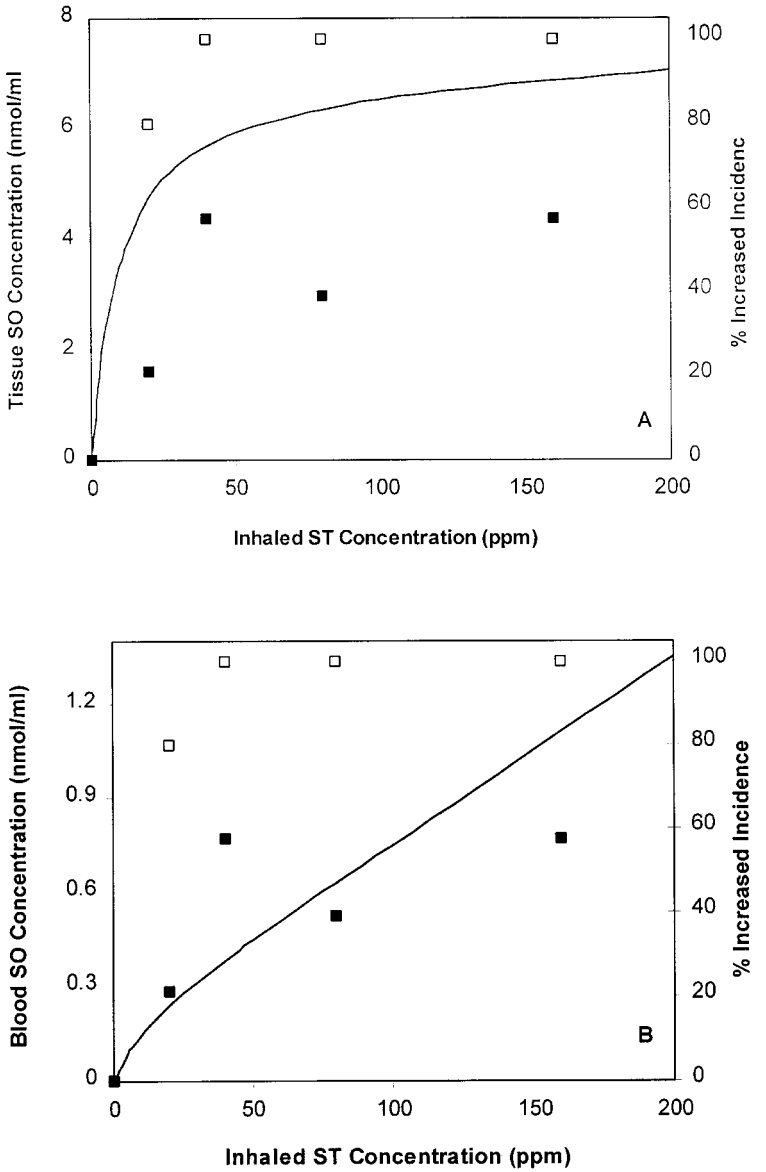

FIGURE 11. Plot comparing model derived steady-state concentration of SO in (top) terminal bronchioles and (bottom) arterial blood in mice following continuous exposure to ST with increased (over background) incidence of neoplastic lesions (adenomas and carcinomas combined) and presursor lesions (neoplastic and preneoplastic combined) in the bronchioloalveolar region in the four ST-exposed groups of males mice (Cruzan et al., 2001). The ST chronic inhalation bioassay results show that the number of male mice at extra risk of developing neoplastic lesions (solid square) in the bronchioloalveolar region is 0%, 21%, 57.6%, 39.4%, and 57.6% and precursor lesions (hollow square) in the bronchioloalveolar region are 0%, 80%, 100%, 100%, and 100% in the control, 20 ppm, 40 ppm, 80 ppm, and 160 ppm dose groups, respectively (Cruzan et al., 2001). Predicted bronchiolar tissue SO concentration shows a better correlation with the tumor incidence compared to systemic SO concentration.

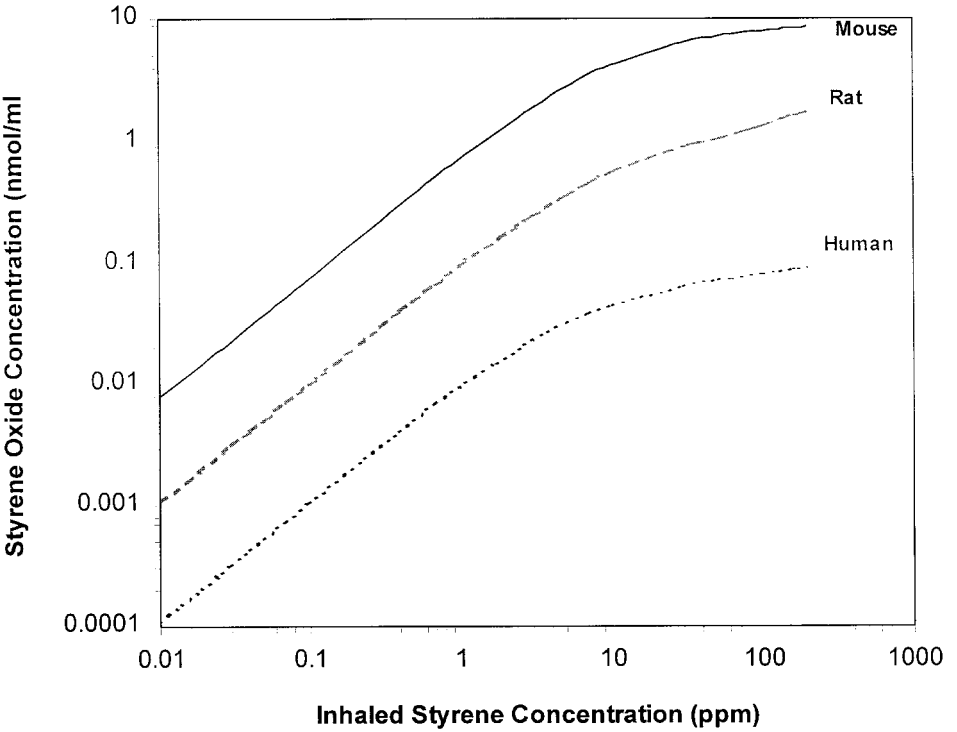

FIGURE 12. Model simulation of steady-state SO concentrations in the terminal bronchioles in mouse (solid line), rat (dashed line), and human (dotted line) for a wide range of inhaled ST concentrations. Tissue SO concentration are predicted to be approximately 10-fold lower in the rat terminal bronchioles compared to the mouse, and 100-fold lower in human transitional bronchioles compared to the mouse. The tissue concentrations reflect P-450 activity in the Clara-cell-rich terminal/transitional bronchioles in all three species.

Compared to the mouse, SO concentrations are approximately 10- and 100-fold lower in the rat and human transitional bronchioles, respectively. These patterns in SO tissue dose metrics are predominantly a reflection of the transitional bronchiolar P-450 activity in the three species (Table 4). Most importantly, model-predicted SO concentration in the rat terminal bronchioles at the highest exposure concentration used in the rat bioassay (1000 ppm) is more than twofold below corresponding mouse target tissue concentration at the lowest tumorigenic exposure in the mouse bioassay (20 ppm). This suggests a pharmacokinetic limitation in the rat that results in tissue doses that are below the lowest tumorigenic dose in the mouse. This is consistent with the observed species sensitivity to inhaled ST. Model simulations also indicate that tissue doses of SO in human transitional bronchioles, even at the highest exposure concentration used in the mouse chronic bioassay, will remain well below the lowest tumorigenic dose in

the mouse. To the extent that the species sensitivity can be attributed solely to pharmacokinetic differences and to tissue dosimetry, humans would be expected to be 100-fold less sensitive to the induction of lung tumors following ST exposure than mice.

R/S SO Tissue Dose Comparison in Rodents

Species differences in susceptibility to ST toxicity have been attributed to quantitative differences in the amount of *R*-SO and *S*-SO in the target tissue following inhalation of ST (Bond, 1989; SIRC, 1999). The simulated steady-state tissue concentrations of *R*-SO and *S*-SO in the terminal bronchiolar compartment in mouse and rat are shown in Table 5b. These simulations are based on the assumption that the stereoselective GST activity in mice lung is same as that measured in rats (see Methods). Model predictions indicate that the concentrations of *R*-SO, the slightly more mutagenic and cytotoxic SO enantiomer, are 2.5-fold higher than *S*-SO in the mouse terminal bronchioles. This trend is reversed in rat terminal bronchioles, where *R*-SO concentrations are approximately 30% lower than *S*-SO concentrations. Furthermore, the maximum *R*-SO concentration attained in rats at the highest exposure concentration (1000 ppm) is less than the *R*-SO concentration in mice at 20 ppm (lowest tumorigenic dose), similar to the trend in total SO tissue dose in the two rodent species. These model simulations indicate that the stereospecific metabolic activation and detoxication of SO may also contribute to the large differences in species sensitivity to ST toxicity.

Alternate Tissue Dose Metrics

SO concentration in the Clara cells is an alternative to region-specific average SO concentration in the terminal bronchioles as a dose metric for interspecies extrapolation. Model-based cell-specific estimates are valid for a homogenous cell population and can be considered as the higher limit for SO concentration in the Clara cells. Model-simulated SO concentrations in rat Clara cells are three times lower than the mouse (Figure 13). SO concentrations are higher in Clara cells than the transitional bronchioles only marginally (25%) in mice and by a much larger percent (300%) in rats (Figure 13). The higher SO concentration in the Clara cell relative to the average concentration in the terminal bronchiolar region is proportional to the difference in P-450 activity in the Clara cells and the terminal/transitional bronchioles. The change in P-450 activity is in turn reflective of the fractional Clara cell volume in the transitional bronchioles in the three species. In mice, approximately 80% of the terminal bronchiolar tissue is Clara cells, resulting in a tissue P-450 activity that is about 25% lower than that in the Clara cells. In rat and human, only 35% and 7.5% of the tissue volume in the transitional bronchioles are due to Clara cells, respectively, resulting in tissue P-450 activity that is approximately 3-fold and 13-fold lower than

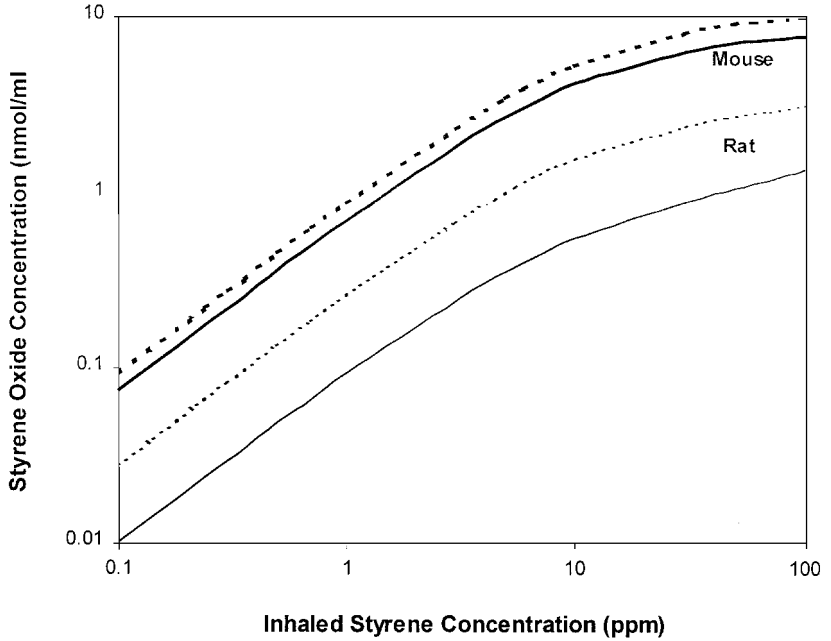

FIGURE 13. Plot comparing region-specific (SO concentration in terminal bronchioles) and cell-specific (Clara cell SO concentration) dose metrics in rats and mice. The SO concentration is approximately 30% higher in Clara cells (dotted line) than the average terminal bronchioles concentration (solid line) in mice, while this difference is about threefold in rats.

Clara-cell activity in the respective species. The predicted difference in tissue dose between the mouse and human, based on pharmacokinetic considerations, will be approximately 10-fold if a Clara cell-specific dose metric is considered for dose extrapolation and 100 if a region-specific dose metric is assumed for dose extrapolation. Hence, the assumption regarding the target cell for carcinogenesis will have a direct and significant impact on the interspecies dose extrapolation.

Determinants of Target Tissue Dose

SO shows significant accumulation in the arterial blood at steady-state. SO concentration in the respiratory-tract compartments is controlled both by local metabolism in the epithelial tissue and by transport of SO into the submucosa from the arterial blood. The impact of systemic delivery of SO on transitional bronchiolar tissue dose can be determined by simulating ST exposures in the absence of hepatic metabolism of styrene (Figure 14). Elimination of hepatic metabolism does not alter the model-based exposure-dose predictions in mouse, but changes the predicted exposure–dose relationship in rat, only at high exposure concentrations.

When similar K_m values are used for P-450-mediated ST metabolism in lung and liver, the predicted SO concentration in respiratory tract tissue

reaches a plateau at lower exposures than the exposures required to cause a plateau in blood SO concentrations. This is because direct air-phase delivery of ST to the lung tissues results in a higher concentration of ST in the respiratory-tract tissues compared to systemic ST concentration. Under this condition of comparable K_ms for P-450 activity in the lung and liver in mice, the relatively high V_{max} for P-450 metabolism in the terminal bronchioles, compared to the liver, results in SO concentrations in the target tissue that are approximately 50-fold higher than blood concentrations for the whole range of tested exposures. Hence, in mice, the respiratory-tract tissue SO concentration is dominated by local production of SO rather than delivery via the arterial blood (Figure 14). In contrast, in rats, the relatively low V_{max} for P-450 metabolism in the terminal bronchioles, compared to the liver, results in target tissue SO concentrations that are higher than blood SO concentrations only for exposures below 50 ppm (Figure 14). Above 50 ppm, hepatic production of SO eventually results in high enough SO blood concentrations leading to increased delivery of SO to the target tissue. Hence, in rats hepatic production of SO can increase respiratory tract tissue concentration at higher exposure concentrations.

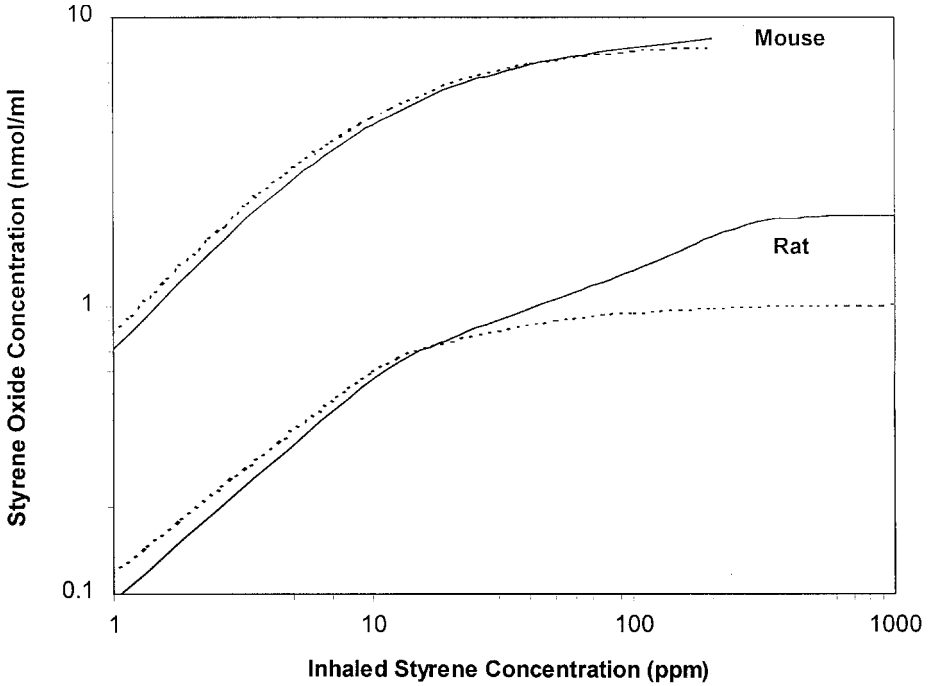

FIGURE 14. Model simulations comparing steady state SO concentration in the terminal bronchioles with (solid line) and without (dotted line) accounting for systemic metabolism (i.e., P-450 activity in the liver) in both mice and rats. In mice, target tissue concentration of SO is determined primarily by air-phase delivery of ST and local metabolism, rather than systemic delivery of ST and SO. In rats, hepatic production of SO can increase respiratory-tract tissue dose at higher exposure concentrations.

Sensitivity Analysis

The various model parameters are not known with absolute certainty. An evaluation of the impact of uncertainty in the parameters on model estimates of tissue dose metrics was obtained by conducting a sensitivity analysis. The analysis was conducted by measuring the change in the tissue dose metric for a pre-specified change in a particular model parameter when all the other parameters were held fixed. The sensitivity coefficients represent the percent change in the venous blood SO concentration or bronchiolar tissue SO concentration for a 1% change in the listed parameter (Table 6). A sensitivity coefficient of 1 indicates that there is a one-to-one correlation between change in the parameter and model output. A positive value for the sensitivity coefficient indicates that the dose metric and the corresponding model parameter are directly correlated, and a negative value indicates they are inversely correlated.

The sensitivity coefficients (SC) for the mouse and human model, as described in Table 6, were calculated at an exposure concentration of 1 ppm using 2 relevant dose metrics: blood SO concentration and transitional bronchiolar SO concentration. The SCs for the two species are qualitatively similar. The SCs for the bronchiolar SO concentration show a high sensitivity

TABLE 6. Sensitivity Analysis in Mice and Human at the Mice LOAEL Concentration (20 ppm) for Two Different Dose Metrics (Blood SO Concentration and Transitional Bronchioles SO Concentration)

	Mouse		Human	
Parameter	[Blood SO]	[Lung SO][a]	[Blood SO]	[Lung SO][a]
Cardiac output	–0.35	–0.8	–0.26	–0.73
Liver blood flow	0.22	—	0.28	—
T. bronchioles blood flow	—	–0.72	—	–0.65
Ventilation rate	0.32	0.22	0.39	0.17
ST blood:air partition coefficient	0.42	0.6	0.47	0.62
SO blood:air partition coefficient	—	—	—	—
Gas-phase MTC	—	—	—	—
Liquid-phase MTC	0.23	–0.16	0.18	–0.06
T. airway tissue thickness	—	0.85	—	0.57
T. airway surface area	—	0.68	—	0.53
V_{max} P-450 liver	—	—	—	—
V_{max} P-450 t. bronchioles	—	0.93	—	0.98
K_m P-450	–0.39	–0.71	–0.44	–0.84
V_{max} EH liver	–0.09	—	–0.46	—
V_{max} EH t. bronchioles	—	–0.09	—	–0.37
K_m EH	0.38	0.09	0.85	0.39
V_{max} GST Liver	–0.27	—	–0.38	—
V_{max} GST t. bronchioles	—	–0.05	—	—
K_{mSO} GST	0.53	0.06	0.43	0.06
K_{mGSH} GST	—	—	—	—
GSH production rate	—	—	—	—

[a]SO concentration in the transitional bronchiolar compartment.

for the local P-450, EH, and GST activity in the lung tissue compartment, while the blood SO concentration is more sensitive to the corresponding parameters in the liver. Apart from enzyme activity, flow parameters such as cardiac output, ventilation rate, and local blood perfusion rate to the target tissue have a high SC since they influence the delivery and clearance of ST and SO from the target site. Furthermore, target tissue thickness and surface area also show a high SC because they determine the transport coefficient of ST and SO across the epithelial tissue into the blood exchange layer. ST blood:air partition coefficient has a high SC since it determines the equilibrium tissue ST concentration for any given inhaled air-phase ST concentration. The remaining model parameters including hepatic activity of phase I and phase II enzymes show negligible sensitivity on the tissue dose metric, reinforcing the conclusion that respiratory-tract tissue concentrations are predominantly shaped by local enzyme activity and flow dynamics.

Due to lack of data, the following assumptions were made in this PBPK model: (1) Tissue:blood partition coefficients in mice and humans were assumed to be the same as in rats, and (2) air-phase MTC of ST and SO was assumed to be equal to the MTC computed using computational fluid dynamics models by Frederick et al. (1998) using acrylic acid, and target-tissue EH affinity (K_m) in mice and humans were assumed to be same as in rats. The sensitivity analysis shows that the assumptions related to air-phase MTC and EH affinity do not have a significant impact on the target-tissue dose metric, whereas the assumption on the tissue:air partition coefficient may result in significant model uncertainty.

DISCUSSION

A number of volatile organic compounds (e.g., butadiene, methylene chloride, trichloroethylene, naphthalene, styrene, etc.) that are metabolized to their reactive intermediates by P-450s in the lung (Clara cells) cause tumors specific to the bronchioloalveolar region in rodents (Cruzan et al., 2001; Green, 2000; Maltoni et al., 1988; Melnick et al., 1993). Most of these compounds also show species-specific differences in the magnitude of the toxicity preceding carcinogenicity or in the incidence of tumors (Cruzan et al., 1998; Maltoni et al., 1988). In the past, PBPK models have been developed to estimate the tissue dose for these inhaled vapors and their metabolites (Andersen et al., 1987; Clewell et al., 2000; Csanady et al., 1994; Sweeney et al., 1996a, 1996b). However, these models have treated the lung as a single homogeneous tissue in equilibrium with arterial blood, and, as a consequence, do not reflect some of the important characteristics of the respiratory tract that control target-tissue dose metrics. These include air-phase delivery of the inhaled volatile to the target tissues, enormous diversity in cell composition and function within the respiratory tract, species differences in the metabolic constants for production (toxication) and clearance (detoxication) of metabolites by Clara cells, and regional Clara-cell density. Lacking

representations of these characteristics, these PBPK models are limited in their ability to predict dosimetry at the target site within the respiratory tract.

The MOA-based PBPK model developed in this report, which has a multicompartment description of the respiratory tract, is a significant advancement over previous ST models This model explicitly incorporates a Clara-cell-rich transitional bronchiolar compartment within the respiratory tract, reflecting the involvement of this specific region of the lung in ST-induced toxicity, as the target tissue. This is particularly important because of the extensive literature describing cell-specific metabolism and toxicity in the transitional bronchioles of the lung for a variety of organics (Green, 1995; Green et al., 1997). Further, this PBPK model accounts for both air-phase and blood-phase delivery of ST and SO to the target tissue. The current multicompartment respiratory-tract model structure can be applied to a whole class of P-450-activated volatiles that elicit a toxic response in the Clara-cell-rich regions of the lung.

Model Uncertainties

The addition and parameterization of the transitional bronchiolar compartment reduce uncertainties implicit in whole-lung models, which ignore large differences in delivery and metabolism of ST/SO at the target region. However, as with most data-intensive PBPK models, there are uncertainties associated with most model parameters some of which can impact the tissue dose predictions. The sensitive model parameters are also the most important entities for further research designed to reduce uncertainty in their estimates. Among the relatively sensitive parameters (sensitivity coefficient > 0.5) in the ST model (Table 6), blood perfusion rate to the target tissue and the target tissue thickness and surface area were parameterized based on available data in the literature and are therefore known with reasonable certainty. The uncertainty associated with these parameters is due to the errors inherent in the measurement process and/or a consequence of intraindividual variations.

Additional uncertainties are attributed to using in vitro measures to make in vivo predictions and the reconstruction of the metabolic parameters from Clara-cell or whole-lung data in the development of the target-tissue specific kinetic constants. The uncertainties for the latter are primarily a result of the uncertainties in the associated data on the cell density. Reported data on Clara-cell density in rat terminal bronchioles range from 25% to 70% (Plopper et al., 1991), and the distribution of Clara cell fraction in mouse conducting airways ranges from 40% to 80% (Parent 1992), indicating an uncertainty of ~2-fold in these parameters. While model estimates of SO concentration in the transitional bronchiolar region cannot be verified due to lack of direct experimental measurements, the physiological and kinetic parameters used to develop model-based estimates are known with reasonable certainty. However, direct experimental measurement of ST and SO concentrations in the Clara-cell-rich regions of the lung and/or indirect measures such as regional ST extraction in the lung or GSH depletion in the tar-

get tissues will help model validation and greatly improve the confidence in the model-based target tissue dose predictions.

The need to account for uncertainty in the cell of origin for the observed tumors created the need to develop the two dose metrics, one that is Clara-cell specific and one that is region specific, to account for the possibility that either Type II cells or Clara cells as the cell of origin for these tumors. This uncertainty directly impacts dosimetry because the predicted dose metrics can vary by 10-fold depending on the cell of origin. Model simulations indicate that Clara-cell SO concentration can be potentially higher than the average tissue concentration in the transitional bronchioles. The benefit of treating this uncertainty explicitly in the model is that the results of additional experimental work on the cell of origin of ST induced bronchiolar alveolar tumors can be used directly to reduce model uncertainty.

Inferences on Species Sensitivity

A principle conclusion of the pharmacokinetic analysis presented here is that integration of available data on the metabolic production and clearance of SO in the transitional bronchioles of rats and mice results in predictions of SO concentrations in rats (insensitive) that cannot reach concentrations equivalent to those in the mouse (sensitive) at the lowest tumorigenic exposure (20 ppm). This pharmacokinetic limitation on tissue dose in the rat is consistent with the observed species sensitivity. Rats do not display toxicity or carcinogenicity at ST concentrations as high as 1000 ppm. Further, the ratio of the slightly more potent enantiomer, *R*-SO, to *S*-SO is lower in the rat than the mouse. This presents a strong case for a pharmacokinetic basis for the observed species differences in ST toxicity. However, it is not possible to attribute the observed species differences in ST-induced lung tumors solely to pharmacokinetics because of the relatively high background incidence of bronchioloalveolar tumors in control mice, which may indicate other pharmacodynamics differences between rats and mice. Both pharmacokinetics and pharmacodynamics should be considered when evaluating the relevance of the mouse results to human risk assessment.

Model Application in Risk Assessment

Default approaches for conducting animal to human dose extrapolations in support of a carcinogen risk assessment tend to be highly conservative. The conservative assumptions assure that virtually safe dose estimates are protective in the presence of substantial uncertainties and limitations in the approaches. These simple empirical approaches are appropriate when insufficient data is available to conduct biologically motivated extrapolations. Mode-of-action-based dosimetry models that utilize anatomical, physiological, and chemical-specific pharmacokinetic data reduce uncertainties associated with extrapolation from high to low dose and from experimental animals to humans. This PBPK model for evaluating respiratory

tract concentration of ST and SO provides a strong foundation for the development of both cancer and noncancer risk assessment for inhaled ST. These modeling results also suggest a pharmacokinetic explanation for species sensitivity from ST-induced toxicity.

As shown in our analysis, local metabolism and direct equilibration of airborne vapors with respiratory-tract tissues are dominant factors controlling tissue doses of metabolites in the mouse at ST exposure levels that lead to bronchioloalveolar carcinogenic. Earlier models for volatile organics, such as the PBPK model for methylene chloride and trichloroethylene (Andersen et al., 1987; Clewell et al., 2000), did not partition the lung into multiple segments based on cell composition to account for local metabolism or provide for airway equilibration and arterial blood delivery of reactive metabolites. These models have guided various risk assessments. These model-based dose-response assessments should be revisited with a more accurate description of respiratory tract structure and metabolism. For volatile toxicants with effects in the respiratory tract, PBPK models intended to support human health risk assessments should use a multicompartment description of the lung that incorporates local metabolism and gas-phase delivery to respiratory-tract epithelium.

Conclusion

We have developed a PBPK model with a multicompartment description of the respiratory tract with a compartment specific to the target tissue for ST toxicity and carcinogenicity, the terminal bronchioles. Parameterization of Phase I and II metabolism in the terminal bronchiolar compartment was derived based on species-specific data on regional distribution of cells in the transitional bronchioles and their respective metabolic activity. The model is validated against in vivo pharmacokinetic data, and used to derive quantitative relationships between exposure concentration of ST and internal tissue dose of SO in mice, rats, and humans. We have also conducted an analysis of *R/S*-SO target-tissue dose following ST exposure in rats and mice using the PBPK model. Compared with the mouse, model-based predictions of SO concentrations are approximately 10- and 100-fold lower in the rat and human transitional bronchioles, respectively. These predictions support a pharmacokinetic basis for species sensitivity in rodents and indicate that humans will be approximately 100-fold less sensitive to the induction of lung tumors following ST exposure than are mice.

REFERENCES

Andersen, M. E., Clewell, H. J. III, Gargas, M. L., Smith, F. A., and Reitz, R. H. 1987. Physiologically based pharmacokinetics and the risk assessment process for methylene chloride. *Toxicol. Appl. Pharmacol.* 87:185–205.

Andersen, M. E., Sarangapani, R., Frederick, C. B., and Kimbell, J. S. 1999. Dosimetric adjustment factors for methylmethacrylate derived from a steady-state analysis of a physiologically based clearance-extraction model. *Inhal. Toxicol.* 11:899–926.

Anttila, S., Hirvonen, A., Vainio, H., Husgafvel-Pursiainen, K., Hayes, J. D., and Ketterer, B. 1993.

Immunohistochemical localization of glutathione *S*-transferases in human lung. *Cancer Res.* 53: 5643–5648.

Baron, J., and Voigt, J. 1990. Localization, distribution, and induction of xenobiotic-metabolizing enzymes and aryl hydrocarbon hydroxylase activity within lung. *Pharmacol. Ther.* 47:419–445.

Barton, H., Deisinger, P., English, J., Gearhart, J., Faber, W., Tyler, T., Banton, M., Teeguarden, J., and Andersen, M. 2000. Family approach for estimating reference concentrations/doses for series of related organic chemicals. *Toxicol. Sci.* 54:251–261.

Birnbaum, L. S., and Baird, M. B. 1979. Senescent changes in rodent hepatic epoxide metabolism. *Chem. Biol. Interact.* 26:245–256.

Bogdanffy, M. S., Sarangapani, R., Kimbell, J. S., Frame, R. S., and Plowchalk, D. R. 1998. Analysis of vinyl acetate metabolism in rat and human nasal tissues by an in vitro gas uptake technique. *Toxicol. Sci.* 46:235–246.

Bogdanffy, M. S., Sarangapani, R., Plowchalk, D. R., Jarabek, A., and Andersen, M. E. 1999. A biologically-based risk assessment for vinyl acetate-induced cancer and non-cancer inhalation toxicity. *Toxicol. Sci.* 51:19–35.

Bond, J. 1989. Review of the toxicology of styrene. *Crit. Rev. Toxicol.* 19:227–249.

Boorman, G. A., Montgomery, C. A., Jr., and MacKenzie, W. F., eds. 1990. *Pathology of the Fischer rat: Reference and atlas.* San Diego: Academic Press.

Brown, R. P., Delp, M. D., Lindstedt, S. L., Rhomberg, L. R., and Beliles, R. P. 1997. Physiological parameter values for physiologically based pharmacokinetic models. *Toxicol. Ind. Health* 13:407–484.

Butler, J., ed. 1992. *The bronchial circulation.* New York: Marcel Dekker.

Carlson, G. 1998. Metabolism of styrene oxide to styrene glycol by mouse liver and lung. *J. Toxicol. Environ. Health* 53:19–27.

Carlson, G., Hynes, D., and Mantick, N. 1998. Effects of inhibitors of CYP1A and CYP2B on styrene metabolism in mouse liver and lung microsomes. *Toxicol. Lett.* 98:131–137.

Chang, H. K., and Paiva, M. 1989. *Respiratory physiology: An analytical approach.* New York: Marcel Dekker.

Clewell, H. J. 3rd, Gentry, P. R., Covington, T. R., and Gearhart, J. M. 2000. Development of a physiologically based pharmacokinetic model of trichloroethylene and its metabolites for use in risk assessment. *Environ. Health Perspect.* 108(suppl. 2):283–305.

Cook, J., Pass, H., Iype, S., Friedman, N., DeGraff, W., Russo, A., and Mitchell, J. 1991. Cellular glutathione and thiol measurements from surgically resected human lung tumor and normal lung tissue. *Cancer Res.* 51:4287–4294.

Coursin, D., Cihla, H., Oberley, T., and Oberley, W. L. 1992. Immunolocalization of antioxidant enzymes and isozymes of glutathione *S*-transferase in normal rat lung. *Am. J. Physiol.* 263:L679–L691.

Cruzan, G., Cushman, J., Andrews, L., Granville, G., Johnson, K., Hardy, C., Coombs, D., Mullins, P., and Brown, W. 1998. Chronic toxicity/oncogenicity study of styrene in CD rats by inhalation exposure for 104 weeks. *Toxicol. Sci.* 46:266–281.

Cruzan, G., Cushman, J. R., Andrews, L. S., Granville, G. C., Johnson, K. A., Bevan, C., Hardy, C. J., Coombs, D. W., Mullins, P. A., and Brown, W. R. 2001. Chronic toxicity/oncogenicity study of styrene in CD-1 mice by inhalation exposure for 104 weeks. *J. Appl. Toxicol.* 21:185–98.

Csanady, G., Mendrala, A., Nolan, R., and Filser, J. 1994. A physiologic pharmacokinetic model for styrene and styrene-7,8-oxide in mouse, rat and man. *Arch. Toxicol.* 68:143–157.

Cussler, E. L. 1999. *Diffusion: Mass transfer in fluid systems.* Cambridge, UK: Cambridge University Press.

Deutschmann, S., and Laib, R. 1989. Concentration-dependent depletion of non-protein sulfhydryl (NPSH) content in lung, heart and liver tissue of rats and mice after acute inhalation exposure to butadiene. *Toxicol. Lett.* 45:175–183.

D'Souza, R. W., Francis, W. R., and Andersen, M. E. 1988. Physiological model for tissue glutathione depletion and increased resynthesis after ethylene dichloride exposure. *J. Pharmacol. Exp. Ther.* 245:563–568.

Filser, J. G., Schwegler, U., Csanady, G. A., Greim, H., Kreuzer, P. E., and Kessler, W. 1993. Species-specific pharmacokinetics of styrene in rat and mouse. *Arch. Toxicol.* 67:517–530.

Frederick, C. B., Bush, M. L., Lomax, L. G., Black, K. A., Finch, L., Kimbell, J. S., Morgan, K. T.,

Subramaniam, R. P., Morris, J. B., and Ultman, J. S. 1998. Application of a hybrid computational fluid dynamics and physiologically based inhalation model for interspecies dosimetry extrapolation of acidic vapors in the upper airways. *Toxicol. Appl. Pharmacol.* 152:211–231.

Gadberry, M., DeNicola, D., and Carlson, G. 1996. Pneumotoxicity and hepatotoxicity of styrene and styrene oxide. *J. Toxicol. Environ. Health* 48:273–294.

Gargas, M. L., Burgess, R. J., Voisard, D. E., Cason, G. H., and Andersen, M. E. 1989. Partition coefficients of low-molecular-weight volatile chemicals in various liquids and tissues. *Toxicol. Appl. Pharmacol.* 98:87–99.

Green, T. 1995. *Methylene chloride induced mouse liver and lung tumours.* Arderley Park, Macclesfield, Cheshire, UK: Zeneca, Central Toxicology Laboratory.

Green, T. 1999. *Styrene: A 10 day inhalation study to investigate effects of mouse and rat lung.* Alderley Park, Macclesfield, Cheshire, UK: Zeneca Central Toxicology Laboratory.

Green, T. 2000. Pulmonary toxicity and carcinogenicity of trichloroethylene: species differences and modes of action. *Environ. Health Perspect.* 108(suppl. 2):261–264.

Green, T., Mainwaring, G. W., and Foster, J. R. 1997. Trichloroethylene-induced mouse lung tumors: Studies of the mode of action and comparisons between species. *Fundam. Appl. Toxicol.* 37:125–130.

Griffeth, L. K., Rosen, G. M., and Rauchman, E. J. 1987. Effects of model traumatic injury on hepatic drug metabolism in the rat. VI. Major detoxification/toxification pathways. *Drug Metab. Dispos.* 15:749–759.

Hiratsuka, A., Yokoi, A., Iwata, H., Watabe, T., Satoh, K., Hatayama, I., and Sato, K. 1989. Glutathione conjugation of styrene 7,8-oxide enantiomers by major glutathione transferase isoenzymes isolated from rat livers. *Biochem. Pharmacol.* 38:4405–4413.

Hynes, D. E., DeNicola, D. B., and Carlson, G. P. 1999. Metabolism of styrene by mouse and rat isolated lung cells. *Toxicol. Sci.* 51:195–201.

ICRP. 1994. *Human respiratory tract model for radiological protection: A report of a task group of the International Commission on Radiological Protection.* Oxford, UK: Elsevier Sciences, Ltd.

Jeffery, P. K., and Reid, L. 1975. New observations of rat airway epithelium: A quantitative and electron microscopic study. *J. Anat.* 120:295–320.

Johanson, G., Ernstgard, L., Gullstrand, E., Lof, A., Osterman-Golkar, S., Williams, C. C., and Sumner, S. C. 2000. Styrene oxide in blood, hemoglobin adducts, and urinary metabolites in human volunteers exposed to (13)C(8)-styrene vapors. *Toxicol. Appl. Pharmacol.* 168:36–49.

Johanson, G., and Filser, J. G. 1992. Experimental data from closed chamber gas uptake studies in rodents suggest lower uptake rate of chemical than calculated from literature values on alveolar ventilation. *Arch. Toxicol.* 66:291–295.

Johanson, G., and Filser, J. G. 1993. A physiologically based pharmacokinetic model for butadiene and its metabolite butadiene monoxide in rat and mouse and its significance for risk extrapolation. *Arch. Toxicol.* 67:151–163.

Jones, K., Holland, J., Foureman, G., Bend, J., and Fouts, J. 1983. Xenobiotic metabolism in Clara cells and alveolar type II cells isolated from lungs of rats treated with beta-naphthoflavone. *J. Pharmacol. Exp. Ther.* 225:316–319.

Linhart, I., Gut, I., Smejkal, J., and Novak, J. 2000. Biotransformation of styrene in mice. Stereochemical aspects. *Chem. Res. Toxicol.* 13:36–44.

Lof, A., Gullstrand, E., Lundgren, E., and Nordqvist, M. B. 1984. Occurrence of styrene-7,8-oxide and styrene glycol in mouse after the administration of styrene. *Scand. J. Work. Environ. Health* 10: 179–187.

Lu, S. C. 1999. Regulation of hepatic glutathione synthesis: current concepts and controversies. *FASEB J.* 13:1169–1183.

Mace, K., Bowman, E. D., Vautravers, P., Shields, P. G., Harris, C. C., and Pfeifer, A. M. 1998. Characterisation of xenobiotic-metabolising enzyme expression in human bronchial mucosa and peripheral lung tissues. *Eur. J. Cancer* 34:914–920.

Maltoni, C., Cotti, G., and Perino, G. 1988. Long-term carcinogenicity bioassays on methylene chloride administered by ingestion to Sprague-Dawley rats and Swiss mice and by inhalation to Sprague-Dawley rats. *Ann. NY Acad. Sci.* 534:352–366.

Massaro, E. J. 1997. *Handbook of human toxicology*. Boca Raton, FL: CRC Press.

McConnell, E., and Swenberg, J. 1994. Review of styrene and styrene oxide long-term animal studies. *Crit. Rev. Toxicol.* 24:S49–S55.

Melnick, R. L., Shackelford, C. C., and Huff, J. 1993. Carcinogenicity of 1,3-butadiene. *Environ. Health Perspect.* 100:227–236.

Menache, M., Hanna, L., Gross, E., Lou, S., Zinreich, S., Leopold, D., Jarabek, A., and Miller, F. 1997. Upper respiratory tract surface areas and volumes of laboratory animals and humans: Considerations for dosimetry models. *J. Toxicol. Environ. Health* 50:475–506.

Mendrala, A. L., Langvardt, P. W., Nitschke, K. D., Quast, J. F., and Nolan, R. J. 1993. In vitro kinetics of styrene and styrene oxide metabolism in rat, mouse, and human. *Arch. Toxicol.* 67:18–27.

Mercer, R. R., Russell, M. L., Roggli, V. L., and Crapo, J. D. 1994. Cell number and distribution in human and rat airways. *Am. J. Respir. Cell Mol. Biol.* 10:613–24.

Miller, R., Newhook, R., and Poole, A. 1994. Styrene production, use, and human exposure. *Crit. Rev. Toxicol.* 24:S1–S10.

Morgan, D. L., Mahler, J. F., Dill, J. A., Price, H. C., Jr., O'Connor, R. W., and Adkins, B., Jr. 1993. Styrene inhalation toxicity studies in mice. III. Strain differences in susceptibility. *Fundam. Appl. Toxicol.* 21:326–333.

Morris, J. B. 2000. Uptake of styrene in the upper respiratory tract of the CD mouse and Sprague-Dawley rat. *Toxicol. Sci.* 54:222–228.

Nakajima, T., Elovaara, E., Gonzalez, F. J., Gelboin, H. V., Raunio, H., Pelkonen, O., Vainio, H., and Aoyama, T. 1994. Styrene metabolism by cDNA-expressed human hepatic and pulmonary cytochromes P450. *Chem. Res. Toxicol.* 7:891–896.

Oesch, F., Zimmer, A., and Glatt, H. R. 1983. Microsomal epoxide hydrolase in different rat strains. *Biochem. Pharmacol.* 32:1783–1788.

Oldham, M., Phalen, R., Schum, G., and Daniels, D. 1994. Predicted nasal and tracheobronchial particle deposition efficiencies for the mouse. *Ann. Occup. Hyg.* 38:135–141.

Pacifici, G. M., Boobis, A. R., Brodie, M. J., McManus, M. E., and Davies, D. S. 1981. Tissue and species differences in enzymes of epoxide metabolism. *Xenobiotica* 11:73–79.

Pacifici, G., Warholm, M., Guthenberg, C., Mannervik, B., and Rane, A. 1987. Detoxification of styrene oxide by human liver glutathione transferase. *Hum. Toxicol.* 6:483–489.

Pacifici, G. M., Franchi, M., Bencini, C., Repetti, F., Di Lascio, N., and Muraro, G. B. 1988. Tissue distribution of drug-metabolizing enzymes in humans. *Xenobiotica* 18:849–856.

Pack, R. J., Al-Ugaily, L. H., and Morris, G. 1981. The cells of the tracheobronchial epithelium of the mouse: A quantitative light and electron microscope study. *J. Anat.* 132:71–84.

Parent, R. A., ed. 1992. *Treatise on pulmonary toxicology*. Boca Raton, FL: CRC Press.

Paulsson, B., Bende, M., and Ohlin, P. 1985. Nasal mucosal blood flow at rest and during exercise. *Acta Otolaryngol.* 99:140–143.

Plopper, C., and Hyde, D. 1992. Epithelial cells of bronchioles. In *Treatise on pulmonary toxicology. Comparative biology of the normal lung,* ed. R. Parent, pp. 131–143. Boca Raton, FL: CRC Press.

Plopper, C. G., Hill, L. H., and Mariassy, A. T. 1980a. Ultrastructure of the nonciliated bronchiolar epithelial (Clara) cell of mammalian lung. III. A study of man with comparison of 15 mammalian species. *Exp. Lung Res.* 1:171–180.

Plopper, C. G., Hyde, D. M., and Buckpitt, A. R. 1991. Clara cells. In *The lung: Scientific foundations,* eds. R. G. Crystal and J. B. West, pp. 517–534. New York: Raven Press.

Plopper, C. G., Macklin, J., Nishio, S. J., Hyde, D. M., and Buckpitt, A. R. 1992. Relationship of cytochrome P-450 activity to Clara cell cytotoxicity. III. Morphometric comparison of changes in the epithelial populations of terminal bronchioles and lobar bronchi in mice, hamsters, and rats after parenteral administration of naphthalene. *Lab. Invest.* 67:553–565.

Plopper, C. G., Mariassy, A. T., and Hill, L. H. 1980b. Ultrastructure of the nonciliated bronchiolar epithelial (Clara) cell of mammalian lung: I. A comparison of rabbit, guinea pig, rat, hamster, and mouse. *Exp. Lung Res.* 1:139–154.

Potter, D. W., and Tran, T. B. 1993. Apparent rates of glutathione turnover in rat tissues. *Toxicol. Appl. Pharmacol.* 120:186–192.

Ramsey, J. C., and Andersen, M. E. 1984. A physiologically based description of the inhalation pharmacokinetics of styrene in rats and humans. *Toxicol. Appl. Pharmacol.* 73:159–175.

Ramsey, J. C., and Young, J. D. 1978. Pharmacokinetics of inhaled styrene in rats and humans. *Scand. J. Work. Environ. Health* 4:84–91.

Sato, A., and Nakajima, T. 1979. A vial-equilibration method to evaluate the drug-metabolizing enzyme activity for volatile hydrocarbons. *Toxicol. Appl. Pharmacol.* 47:41–46.

Schladt, L., Thomas, H., Hartmann, R., and Oesch, F. 1988. Human liver cytosolic epoxide hydrolases. *Eur. J. Biochem.* 176:715–723.

Seidegard, J., DePierre, J. W., Moron, M. S., Johannesen, K. A., and Ernster, L. 1977. Characterization of rat lung epoxide (styrene oxide) hydrase with a modified radioactive assay of improved sensitivity. *Cancer Res.* 37:1075–1082.

SIRC. 1999. *A toxicological review of styrene.* Arlington, VA: U.S. EPA NCEA.

Smith, B. R., Maguire, J. H., Ball, L. M., and Bend, J. R. 1978. Pulmonary metabolism of epoxides. *Fed. Proc.* 37:2480–4284.

Stone, K. C., Mercer, R. R., Gehr, P., Stockstill, B., and Crapo, J. D. 1992. Allometric relationships of cell numbers and size in the mammalian lung. *Am. J. Respir. Cell Mol. Biol.* 6:235–243.

Stoner, G. D. 1998. Introduction to mouse lung tumorigenesis. *Exp. Lung Res.* 24:375–383.

Stott, W., Dryzga, M., and Ramsey, J. 1983. Blood-flow distribution in the mouse. *J. Appl. Toxicol.* 3:310–312.

Stott, W. T., Ramsey, J. C., and McKenna, M. J. 1986. Absorption of chemical vapors by the upper respiratory tract of rats. In *Toxicology of the nasal passages,* ed. C. S. Burrows, pp. 191–210. Washington, DC: Hemisphere.

Sumner, S., and Fennell, T. 1994. Review of the metabolic fate of styrene. *Crit. Rev. Toxicol.* 24:S11–S33.

Sweeney, L. M., Himmelstein, M. W., Schlosser, P. M., and Medinsky, M. A. 1996a. Physiologically based pharmacokinetic modeling of blood and tissue epoxide measurements for butadiene. *Toxicology* 113:318–21.

Sweeney, L. M., Shuler, M. L., Quick, D. J., and Babish, J. G. 1996b. A preliminary physiologically based pharmacokinetic model for naphthalene and naphthalene oxide in mice and rats. *Ann. Biomed. Eng.* 24:305–320.

U.S. Environmental Protection Agency. 1994. *Methods for derivation of inhalation reference concentrations and application of inhalation dosimetry.* Washington, DC: Office of Health and Environmental Assessment.

U.S. Environmental Protection Agency. 1996. *Proposed guidelines for carcinogen risk assessment.* Washington, DC: Office of Research and Development.

U.S. Environmental Protection Agency. 1999. *Review of the USEPA 1996 proposed guidelines for carcinogen risk assessment.* Prepared by Science Advisory Board. Washington, DC: Office of Research and Development.

Waechter, F., Bentley, P., Bieri, F., Muakkassah-Kelly, S., Staubli, W., and Villermain, M. 1988. Organ distribution of epoxide hydrolases in cytosolic and microsomal fractions of normal and nafenopin-treated male DBA/2 mice. *Biochem. Pharmacol.* 37:3897–3903.

Watabe, T., Ozawa, N., and Hiratsuka, A. 1983. Studies on metabolism and toxicity of styrene—VI. Regioselectivity in glutathione *S*-conjugation and hydrolysis of racemic, *R*- and *S*-phenyloxiranes in rat liver. *Biochem. Pharmacol.* 32:777–785.

Wenker, M. A., Kezic, S., Monster, A. C., and de Wolff, F. A. 2000. Metabolism of styrene-7,8-oxide in human liver in vitro: Interindividual variation and stereochemistry. *Toxicol. Appl. Pharmacol.* 169: 52–58.

Withey, J. R., and Collins, P. G. 1979. The distribution and pharmacokinetics of styrene monomer in rats by the pulmonary route. *J. Environ. Pathol. Toxicol.* 2:1329–1342.

Yeh, H. C., and Schum, G. M. 1980. Models of human lung airways and their application to inhaled particle deposition. *Bull. Math. Biol.* 42:461–480.

Yeh, H. C., Schum, G. M., and Duggan, M. T. 1979. Anatomic models of the tracheobronchial and pulmonary regions of the rat. *Anat. Rec.* 195:483–492.

APPENDIX

P-450 Activity in Transition (T.) Bronchioles (Clara-Cell-Rich Region of the Lung) in Mice

1. Data from Hynes et al. (1999) on mouse P-450 activity:

Species	*R*-SO Activity (pmol/min/10^6 Clara cells)	*S*-SO Activity (pmol/min/10^6 Clara cells)	Total lung activity (pmol/min/10^6 Clara cells)
Mouse	152	41.5	193.5

2. Average volume of Clara cell in mice = 420 μm^3 = 420 × 10^{-12} ml (Mercer et al., 1994).
3. Total P-450 activity on a per ml Clara cell basis = (193.5 × 10^{-12} mol/min)/(10^6 cells × 420 × 10^{-12} ml/cell) = 460.7 nmol/min/ml Clara cell.
4. Fraction of Clara cells in T. bronchioles based on cell population density = 78.5% (Plopper & Hyde, 1992).
5. Total P-450 activity on a per ml T. bronchioles tissue basis = 0.785 x 460.7 = 362 nmol/min/ml tissue.

P-450 Activity in Transitional (T.) Bronchioles (Clara-Cell-Rich Region of the Lung) in Rats

1. Data from Hynes et al. (1999) on rat P-450 activity:

Species	*R*-SO Activity (pmol/min/10^6 Clara cells)	*S*-SO Activity (pmol/min/10^6 Clara cells)	Total lung activity (pmol/min/10^6 Clara cells)
Rat	30.1	29	59.1

2. Average volume of Clara cell in rat = 420 × 10^{-12} ml (Mercer et al., 1994).
3. Total P-450 activity on a per ml Clara cell basis = (59.1 × 10^{-12} mol/min)/(10^6 cells × 420 × 10^{-12} ml/cell) = 140.7 nmol/min/ml Clara cell.
4. Fraction of Clara cells in T. bronchioles based on cell population density = 33.0% (Jeffery & Reid, 1975).
5. Total P-450 activity on a per ml T. bronchioles tissue basis = 0.33 × 140.7 = 46.4 nmol/min/ml tissue.

P-450 Activity in Transitional (T.) Bronchioles (Clara-Cell-Rich Region of the Lung) in Humans

1. Data from Nakajima et al. (1994):

Species	P-450 Activity (nmol/min/mg protein)	Protein content[a] (mg protein/ml tissue)	Lung P-450 activity (nmol/min/ml lung tissue)
Human	6.5×10^{-3}	3.8	24.7×10^{-3}

[a]Pacifici et al. (1988).

2. Total Clara cells in human lung = 1380×10^6 cells/lung (Mercer et al., 1994). Total Clara cells in Bronchi = 230×10^6. Total Clara cells in T. bronchioles = 1150×10^6. Average volume of human Clara cell = 400×10^{-12} ml/cell (Mercer et al., 1994).
3. Total Clara cell volume = (1380×10^6 cells/lung) (400×10^{-12} ml/cell) = 0.55 ml.
4. Lung weight (as fraction of body weight) = 0.73% (Brown et al., 1997).
5. Average lung weight in humans (adult) = (0.0073) (70000 g) = 511 g.
6. P-450 activity on ml Clara cell basis = (24.7×10^{-12} mol/min/ml lung tissue) (511 ml/lung)/(0.55 ml) = 22.95 nmol/min/ml Clara cell.
7. Clara cells are present in respiratory bronchioles in humans (i.e., generations 16, 17, and 18): total surface area of R. bronchioles in humans = 6220 cm^2 (Yeh & Schum, 1980).
8. Average cell height in R. bronchioles = 10 μm (Mercer et al., 1994).
9. Average volume of R. bronchioles = 6220 $cm^2 \times 10$ μm = 6.2 ml.
10. Average volume of Clara cells in R. bronchioles = (1150×10^6 cells) (400×10^{-12} ml/cell).
11. P-450 activity on ml R. bronchioles tissue basis = 22.95 nmol/min/ml Clara cells (0.46 ml)/(6.2 ml) = 1.7 nmol/min/ml tissue.